Robotica (2016) volume 34, pp. 1464–1485. © Cambridge University Press 2014
doi:10.1017/S0263574714002392

Adaptive hybrid suppression control of space free-flying robots with flexible appendages

P. Zarafshan†*, S. Ali A. Moosavian‡, and E. G. Papadopoulos§

† *Department of Agro-Technology, College of Aburaihan, University of Tehran, Pakdasht, Tehran, Iran*
‡*Center of Excellence in Robotics and Control, Advanced Robotics and Automated Systems Lab, Department of Mechanical Engineering, K. N. Toosi University of Technology, Tehran, Iran*
§*Department of Mechanical Engineering, National Technical University of Athens, Athens, Greece*

(Accepted Aug 18, 2014. First published online: September 17, 2014)

SUMMARY
Control of rigid–flexible multi-body systems in space, during cooperative manipulation tasks, is studied in this paper. During such tasks, flexible members such as solar panels may vibrate. These vibrations in turn can lead to oscillatory disturbing forces on other subsystems, and consequently may produce significant errors in the position of operating end-effectors of cooperative arms. Therefore, to design and implement efficient model-based controllers for such complicated nonlinear systems, deriving an accurate dynamics model is required. On the other hand, due to practical limitations and real-time implementation, such models should demand fairly low computational complexity. In this paper, a precise dynamics model is derived by virtually partitioning the system into two rigid and flexible portions. These two portions will be assembled together to generate a proper model for controller design. Then, an adaptive hybrid suppression control (AHSC) algorithm is developed based on an appropriate variation rule of a virtual damping parameter. Finally, as a practical case study a space free-flying robot (SFFR) with flexible appendages is considered to move an object along a desired path through accurate force exertion by several cooperative end-effectors. This system includes a main rigid body equipped with thrusters, two solar panels, and two cooperative manipulators. The system also includes a third and fourth arm that act as a communication antenna and a photo capturing camera, respectively. The maneuver is deliberately planned such that flexible modes of solar panels get stimulated due to arms motion, while obtained results reveal the merits of proposed controller as will be discussed.

KEYWORDS: Space robotic; Rigid–flexible multi-body systems; Adaptive control; Dynamics modeling; Suppression control.

Nomenclature

a = Cross sectional area of flexible member	(m^2)
$\mathbf{B}_f$ = Virtual damping matrix of flexible member	(N.s/m)
$\hat{\mathbf{B}}_f$ = Estimated virtual damping matrix of flexible member	(N.s/m)
$\tilde{\mathbf{B}}_f$ = Error in estimated virtual damping matrix of flexible member	(N.s/m)
$\mathbf{C}$ = Vector of quadratic nonlinear velocity terms	(N, N.m)
EI = Bending stiffness of flexible member	($N.m^2$)
$\mathbf{G}$ = Vector of gravity force effects	(N, N.m)
$\underline{\mathbf{G}}$ = Grasp matrix	
$\mathbf{H}$ = The system mass matrix (Positive definite)	($kg, kg.m^2$)

* Corresponding author. E-mail: p.zarafshan@ut.ac.ir

Nomenclature

I = Identity matrix
$\mathbf{J}_c$ = Jacobian matrix for the manipulators (m)
$\mathbf{J}_f$ = Jacobian matrix of floating frame corresponding to each flexible body (m)
$\mathbf{K}$ = Stiffness matrix of flexible member (N/m)
$\underline{\mathbf{K}}$ = Regressor matrix
$\mathbf{K}_p$, $\mathbf{K}_d$ = Controller gain matrices for the object motion
$\tilde{\mathbf{K}}_p$, $\tilde{\mathbf{K}}_d$ = Controller gain matrices for the whole system in the task space
$\mathbf{K}_{PZ}$ = Capacitance matrix for the piezoelectric patches (N/V)
L_b = Length of flexible members (m)
$m^{\{i\}}$ = Mass of the {i}-th flexible body (kg)
$\mathbf{M}_f$ = Positive definite mass matrix of flexible member (kg, kg.m^2)
n_b = Number of flexible members
$\mathbf{q}$ = Vector of generalized coordinates of rigid subsystem (m, deg)
$\bar{\mathbf{q}}$ = Vector of generalized coordinates of flexible subsystem
$\bar{\mathbf{q}}_f$ = Vector of elastic generalized coordinates of flexible subsystem
$\bar{\mathbf{q}}_r$ = Vector of reference or rigid generalized coordinates of flexible subsystem
$\mathbf{Q}$ = Vector of generalized forces (N, N.m)
$\mathbf{Q}_e$ = Vector of generalized external forces of flexible member (N, N.m)
$\tilde{\mathbf{Q}}_f$ = Vector of control forces for object motion (N, N.m)
$\mathbf{Q}_{flex.}$ = Vector of generalized forces due to stimulation of the flexible members (N, N.m)
$\tilde{\mathbf{Q}}_m$ = Vector of control forces for end-effector motion (N, N.m)
$\tilde{\mathbf{Q}}_{react}$ = Vector of reaction forces in task space exerted from object to end-effectors (N, N.m)
$\tilde{\mathbf{Q}}_{supp.}$ = Vector of suppression forces in task space to control flexible member (N, N.m)
$\mathbf{Q}_v$ = Quadratic velocity vector of flexible member (N, N.m)
$\underline{\mathbf{Q}}$, $\underline{\boldsymbol{\rho}}$ = Symmetric positive definite matrices
$\mathbf{R}_{C_0}, \dot{\mathbf{R}}_{C_0}, \ddot{\mathbf{R}}_{C_0}$ = Vector of position, velocity and acceleration of the base CM (m, m/s, m/s^2)
$\mathbf{S}$ = Shape function for flexible member
T = Kinetic energy (J)
$\bar{\mathbf{u}}_f$ = Displacement field of flexible body (m)
$\mathbf{v}_a$ = Vector of voltages for flexible member actuators (V)
V, M = Shear force and bending moment corresponding to flexible member (N, N.m)
$\mathbf{V}$ = Lyapunov function
$\mathbf{x}$, $\dot{\mathbf{x}}$ = Vector of object position, and its rate (m,m/sec)
$\mathbf{X}^{(i)}$, $\dot{\mathbf{X}}^{(i)}$ = Position vector of the (i)-th end-effector, and its rate (m,m/sec)
$\underline{\mathbf{Y}}$ = Filtered output in state space form
$\boldsymbol{\beta}_0$ = Euler angles of the robot rigid base (deg)
$\boldsymbol{\delta}_0$ = Orientation of the body reference frame (deg)
$\boldsymbol{\theta}$ = Joints variables vector (deg)
ρ = Mass density of flexible member (kg/m^3)
$\boldsymbol{\sigma}$ = Stress vector of flexible member (N/m^2)
$\boldsymbol{\omega}$ = Angular velocity (rad/sec)
ξ = Dimensionless length of the flexible member
$\boldsymbol{\Gamma}$ = Gain matrix for the adaptation law

Superscript
$\{i\}$ = ith flexible member
(i) = ith rigid member
m = Number of the flexible coordinates
n = Number of the joint space coordinates
p = Number of the work space coordinates

Subscript
f = Flexible part of the system
r = Rigid part of the system
0 = The base body

https://doi.org/10.1017/S0263574714002392 Published online by Cambridge University Press

1. Introduction

Robotic systems are widely used in unsafe, costly and repetitive tasks in terrestrial and space applications.[1] Most available robotic systems are designed such that they can provide essential stiffness for end-effector to reach its desired position without potential deviations due to flexible deformations. This stiffness is usually attained by massive parts. However, design and use of weighty rigid members usually contradicts optimal energy consumption and high speed operation. In particular, for space and on orbit applications a minimum weight design is required which does not tolerate using stiff and rigid members.[2,3] In fact, SFFR have been proposed for on orbit missions in which the base body is a satellite with limited mass equipped with continuous thrusters. Consequently, it does definitely respond freely to dynamic reaction forces due to manipulator or appendage motions. Hence, to control such a system, it is essential to consider the dynamic coupling between manipulators/appendages and its base. On the other hand, the existence of flexible components such as solar panels in SFFR, necessitates considering corresponding effects. The time required for settling the vibration of such parts may delay the operation, and therefore does not allow for increased time efficiency of the system. This conflict between high speed and high accuracy during any operation makes the control of these robots a challenging research problem.[4]

Robotic systems with flexible components are continuous dynamic systems that are usually modeled using a finite number of rigid degrees of freedom, and a limited number of modes. These models are described by a set of ordinary and partial deferential equations, which are usually nonlinear and coupled. Precise solution of these systems in most cases is almost impossible.[5] In studying these systems, if we ignore the flexibility effects, two types of error will be produced. The first one is related to the actuator torques, and the second one corresponds to the position of end-effectors.[6,7] The position/orientation of end-effectors for precise tasks should not experience any vibration even with small amplitude. Therefore, to achieve high accuracy, we must begin with more precise mathematic models.[8–10] In this regard, control of rigid–flexible multi-body systems is currently an attractive research subject because of its application in the articulated space structures and flexible field mobile robotic systems.[11–13] This depends on determining the actuator torques that can produce the desired motion of such a complicated multi-body system. In other words, the inverse dynamics is part of the controller design, though control inputs can be directly applied on a physical system without using a numerical model.[14,15] In fact, operational problems with robotic systems due to structural flexibility lead to subsequent difficulties with their position control.[16] Also, vibration control of space systems with flexible portions has been studied.[17] Attitude control of such systems in the presence of the aforementioned vibrations has been discussed also.[18] The position-force hybrid control is another challenging problem for space robotic systems with flexible bodies which are addressed in some researches. For instance, an adaptive robust control strategy has been introduced to control position and force tracking of a flexible link.[19] Also, an adaptive impedance algorithm to control the end-effectors of a space flexible manipulator has been proposed.[20] However, force interaction with the environment, which is the main focus of this paper, results in a more challenging problem than that of position control of such systems. In fact, the object manipulation operation by rigid–flexible multi-body systems is a problem that has not received much attention in the literature. Of course, the various control algorithms were presented for the object manipulation task performed by rigid robotic systems, i.e. multiple impedance control (MIC),[21] augmented object control,[22] and non-model based impedance control.[23] Although the capabilities of each of these algorithms were demonstrated in the case of rigid systems, their performance must be investigated in the case of rigid–flexible multi-body systems. Since the MIC algorithm has appeared more efficient, its basic concepts will be considered in this paper to be extended for rigid–flexible multi-body robotic systems. The principal concept is that the robot base as the main body, the end-effectors, and the manipulated object itself must be controlled properly for cooperative object manipulation, while stimulation of the flexible appendages should be avoided. To this end, the MIC algorithm is extended for flexible multi-body space robots, using a modification term, added to the control law. This term compensates disturbing forces exerted to the rigid subsystems.[11] In addition, a hybrid position-force control strategy has been studied for space robots.[12] In this hybrid control strategy, a virtual damping is included in the control law which leads to the leaner dynamic of the error. Also, obtaining an optimum amount for the virtual damping in a flexible field mobile robotic system has been addressed.[13] This value for the virtual damping does in turn result in more reduction of flexible solar panels oscillations.

https://doi.org/10.1017/S0263574714002392 Published online by Cambridge University Press

In this paper, first the system dynamics is virtually partitioned into two portions; i.e. rigid and flexible parts, and a proper model for control purposes of rigid–flexible multi-body systems is developed. To perform a cooperative object manipulation task, a hybrid suppression control (HSC) is studied. Based on the developed HSC, an AHSC is proposed to improve the system performance. Using a comprehensive simulation routine, a cooperative object manipulation operation is studied. A model of a SFFR is developed which contains a rigid main body equipped with two manipulating arms and two flexible solar panels, while a third and fourth arm (appendage) are also mounted on the base, i.e. a communication antenna and a photo capturing camera. Obtained results of the model verification and implementations of the proposed controllers are discussed. These results reveal that vibration of the flexible solar panels can produce undesirable errors of the end-effectors. These effects are significantly eliminated by application of the proposed AHSC algorithm, while the manipulation task is accurately performed.

2. Dynamics Modeling

To study the dynamics of a rigid–flexible multi-body system, an inertial frame is used as a universal reference frame. Moreover, body fixed intermediate reference frames are attached to each flexible member or rigid bodies, which are usually called floating frame. Motions relative to this intermediate frame for flexible members occur only due to body deformations. This selection simplifies the calculations of internal forces, since the stress magnitude or corresponding strain does not vary in a rigid body motion. To develop a dynamics model of such systems, various approaches have been used, including Lagrange method,[8,24] Hamilton principal,[25] Newton–Euler equations,[26] the virtual work principle,[27] and Kane's method.[28] On the other hand, controller design for rigid–flexible multi-body systems requires development of proper dynamics model of those. Such models should be as concise as possible for implementation of model-based control algorithms. In most researches on dynamics analyses, the modeling approach introduces an accumulation in the dynamics of rigid–flexible multi-body systems,[29,30] while the resulting models require heavy computations and cannot be practically used for model based controller implementations. In fact, to avoid accumulation in the dynamic model, there are some approaches which model the entire system by virtual partitioning between the rigid and flexible subsystems. In this regard, a hybrid parallelizable low-order algorithm has been presented for multiple rigid body systems.[31] Also, a structural dynamics analysis has been developed by component mode synthesis.[32] The component mode synthesis involves division of a flexible structure into components, definition of sets of component modes, and coupling of the component mode models to form a reduced-order system model. Furthermore, to model a system of flexible and rigid members, one may develop a set of partial differential equations and ordinary differential equations.[33] In this approach, the interface or coupling conditions through the constraint forces should be carefully arranged, where complex mathematical considerations may be required such as using perturbation techniques. For instance, the constraint forces between the rigid and the flexible members have been estimated using a hybrid fuzzy neural system.[34] Moreover, rigid–flexible interactive modeling (RFIM) approach has been recently proposed for dynamics modeling of multi-body systems that decouples motion equations of rigid members from those of flexible members.[35] Using this approach, simpler sets of dynamics equations will be achieved so that obtained model can be used for implementation of model-based controllers. In this section, the RFIM approach is briefly described. To this end, using floating frames under the assumption of large displacements and rotations, the situation of each flexible body in the multi-body system is specified by two sets of reference and elastic variables. The reference variables define the situation and the orientation of the considered body assuming a rigid body motion, while the elastic coordinates describe the body deformations relative to the body reference. To avoid computational difficulties associated with infinite-dimensional spaces, the latter is introduced using classical approximation techniques such as Rayleigh–Ritz method.[14] So, the kinetic energy of a flexible body is developed and the inertia coupling between the reference motion and the elastic deformation is determined. Subsequently, the dynamics equations of the flexible members can be obtained as:

$$\mathbf{M}_{\mathrm{f}}^{\{i\}}\ddot{\bar{\mathbf{q}}}^{\{i\}}+\mathbf{K}^{\{i\}}\bar{\mathbf{q}}^{\{i\}}=\mathbf{Q}_{\mathrm{e}}^{\{i\}}+\mathbf{Q}_{\mathrm{v}}^{\{i\}},\quad \{i\}=\{1,2,\ldots,\quad n_{\mathrm{b}}\}, \tag{1}$$

https://doi.org/10.1017/S0263574714002392 Published online by Cambridge University Press

where n_b is the total number of the flexible bodies in the multi-body system. Also, $\mathbf{Q}_v^{\{i\}} \in \Re^m$ and $\mathbf{Q}_e^{\{i\}} \in \Re^m$ are correspondingly a quadratic velocity vector which contains all gyroscopic and Coriolis components and the vector of generalized forces associated with the $\{i\}$ th body. Moreover, $\mathbf{M}_f^{\{i\}} \in \Re^{m\times m}$ and $\mathbf{K}^{\{i\}} \in \Re^{m\times m}$ are respectively recognized as the symmetric mass matrix and the symmetric positive definite stiffness matrix of the body {i}. It is recommended that $\dot{\bar{\mathbf{q}}}^{\{i\}} \in \Re^m$ is the vector of reference and elastic coordinates of the flexible body. This equation can be written in a partitioned matrix form as:

$$\begin{bmatrix} \mathbf{m}_{rr}^{\{i\}} & \mathbf{m}_{rf}^{\{i\}} \\ \mathbf{m}_{fr}^{\{i\}} & \mathbf{m}_{ff}^{\{i\}} \end{bmatrix} \begin{bmatrix} \ddot{\bar{\mathbf{q}}}_r^{\{i\}} \\ \ddot{\bar{\mathbf{q}}}_f^{\{i\}} \end{bmatrix} + \begin{bmatrix} 0 & 0 \\ 0 & \mathbf{k}_{ff}^{\{i\}} \end{bmatrix} \begin{bmatrix} \bar{\mathbf{q}}_r^{\{i\}} \\ \bar{\mathbf{q}}_f^{\{i\}} \end{bmatrix} = \begin{bmatrix} (\mathbf{Q}_e^{\{i\}})_r \\ (\mathbf{Q}_e^{\{i\}})_f \end{bmatrix} + \begin{bmatrix} (\mathbf{Q}_v^{\{i\}})_r \\ (\mathbf{Q}_v^{\{i\}})_f \end{bmatrix}, \tag{2}$$

where *r* and *f*, respectively, refer to rigid and flexible coordinates of the flexible members. The proposed RFIM approach separates dynamics modeling of the flexible members and the rigid elements of a unified total system.[35] Then, the coupling between these two sets of equations is realized by the kinematics constraints so that the two sets of equations are simultaneously solved. So, if we suppose that the motion's equations of the rigid mobile subsystem can be modified as:[36]

$$\mathbf{H}(\mathbf{q})\,\ddot{\mathbf{q}} + \mathbf{C}(\mathbf{q}, \dot{\mathbf{q}}) + \mathbf{G}(\mathbf{q}) = \mathbf{Q}(\mathbf{q}) + \mathbf{Q}_{\text{flex.}}(\mathbf{q}), \tag{3}$$

where $\mathbf{q} \in \Re^n$ describes the generalized coordinates corresponding to the rigid subsystem, $\mathbf{C}$, $\mathbf{G}$, $\mathbf{Q} \in \Re^n$, and $\mathbf{H} \in \Re^{n\times n}$ are the corresponding vector of nonlinear velocity terms, vector of gravity related terms, generalized forces, and the mass matrix, respectively, and $\mathbf{Q}_{\text{flex.}}(\mathbf{q}) \in \Re^n$ is the generalized forces due to the stimulation of the flexible members which are applied on the rigid subsystem as the modification term or the constraint force. Considering Eq. (2), this term can be achieved as:

$$\mathbf{Q}_{\text{flex.}}(\mathbf{q}) = \sum_{\{i\}=\{1\}}^{\{n_b\}} \mathbf{J}_f^{\{i\}^T} (\mathbf{Q}_e^{\{i\}})_r, \tag{4}$$

where $\mathbf{J}_f^{\{i\}} \in \Re^{6\times 6}$ is the Jacobian matrix of the floating frame of each flexible body related to the inertial frame of the main body. This matrix is a function of the position and the orientation of the flexible body frame with respect to the main body frame. In other words, it describes the position and configuration that the flexible member is installed on the main body. As detailed above, the RFIM approach combines the Lagrange and Newton–Euler methods. To use the RFIM approach, the computation procedure at each time step includes the following calculations as shown in Fig. 1. First, the motion's equations of the rigid subsystem or Eq. (3) are solved, and the acceleration, velocity and position terms of the rigid subsystem, i.e. $\ddot{\mathbf{q}}$, $\dot{\mathbf{q}}$, $\mathbf{q}$ in the above formulation, are calculated. Then, the rigid components of the acceleration, velocity and position terms of each flexile body, i.e. $\ddot{\bar{\mathbf{q}}}_r^{\{i\}}$, $\dot{\bar{\mathbf{q}}}_r^{\{i\}}$, $\bar{\mathbf{q}}_r^{\{i\}}$ in the above formulation, are computed and inserted into the motion equations of the flexible members as input terms. The relationship between these two sets of variables is established by the kinematics constraints between the origin of the floating frame which is attached to the flexible member and the reference frame of the rigid subsystem. Considering these inputs, the second row of Eq. (2) is solved, and the flexible components of the acceleration, velocity and position terms of each flexile body, i.e. $\ddot{\bar{\mathbf{q}}}_f^{\{i\}}$, $\dot{\bar{\mathbf{q}}}_f^{\{i\}}$, $\bar{\mathbf{q}}_f^{\{i\}}$ in the above formulation, are calculated. Using these values, and substituting into the first row of Eq. (2), the constraint forces or $\mathbf{Q}_e^{\{i\}}$ are computed. Also, using Eq. (4) these results determine the forces produced from vibration of flexible members, which are applied to the equations of the rigid subsystem as $\mathbf{Q}_{\text{flex.}}(\mathbf{q})$ in Eq. (3). In the next sections, the HSC and the AHSC algorithm are developed for a cooperative object manipulation using the RFIM approach.

3. Hybrid Suppression Control

To perform a cooperative object manipulation task by rigid–flexible robotic systems, the flexible members must be controlled to minimize the disturbance forces which are produced from vibration or fast dynamics of these flexible members. Also, in order to complete a successful operation it is

https://doi.org/10.1017/S0263574714002392 Published online by Cambridge University Press

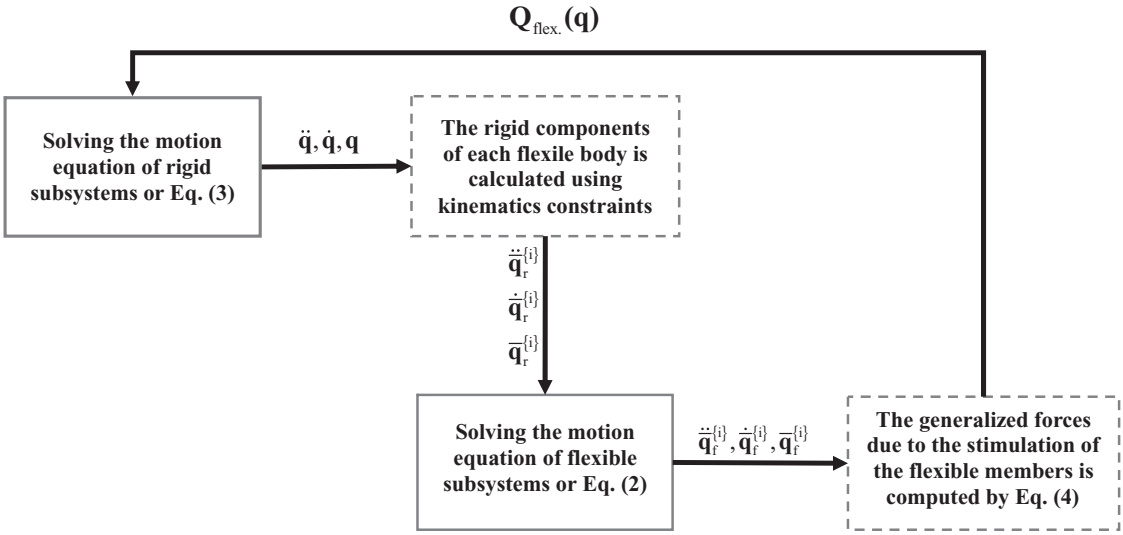

Fig. 1. The block diagram of the rigid–flexible interactive dynamics modeling approach.

necessary to have a more precise control on the members, which are involved in the task. So, these two aspects should be considered in a successful control strategy as proposed here. In fact, in HSC of oscillations of flexible members are controlled to reduce disturbances on the rigid subsystem, leading to a successful object manipulation operation. To this end, the obtained motion's equations of the robotic system or Eq. (3) can be written in the task space or $\tilde{\mathbf{X}}^{(i)} \in \Re^{p}$ as:

$$\tilde{\mathbf{H}}^{(i)}(\mathbf{q}^{(i)})\ddot{\tilde{\mathbf{X}}}^{(i)} + \tilde{\mathbf{C}}^{(i)}(\mathbf{q}^{(i)}, \quad \dot{\mathbf{q}}^{(i)}) = \tilde{\mathbf{Q}}^{(i)} + \tilde{\mathbf{Q}}_{\text{flex.}}^{(i)}, \tag{5}$$

where (i) indicates the (i)th manipulator and:

$$\begin{aligned} \tilde{\mathbf{H}}^{(i)} &= \mathbf{J}_{c}^{(i)^{-T}} \mathbf{H}^{(i)} \mathbf{J}_{c}^{(i)^{-1}} \\ \tilde{\mathbf{C}}^{(i)} &= \mathbf{J}_{c}^{(i)^{-T}} \mathbf{C}^{(i)} - \tilde{\mathbf{H}}^{(i)} \dot{\mathbf{J}}_{c}^{(i)} \dot{\mathbf{q}}^{(i)} \\ \tilde{\mathbf{Q}}^{(i)} &= \mathbf{J}_{c}^{(i)^{-T}} \mathbf{Q}^{(i)}, \quad \tilde{\mathbf{Q}}_{\text{flex.}}^{(i)} = \mathbf{J}_{c}^{(i)^{-T}} \mathbf{Q}_{\text{flex.}}^{j} \end{aligned}, \tag{6}$$

where $\mathbf{J}_{c}^{(i)} \in \Re^{p \times n}$ is a Jacobian matrix for the (i)-th manipulator. Also, $\tilde{\mathbf{X}}^{(i)}$ is the vector of output coordinates or task space coordinates. So, it is considered as the generalized coordinates of the robot base and end-effectors in this object manipulation operation. The main principle of the MIC,[21] is that the robot base, end-effectors, and the object must be moved accordingly for cooperative object manipulation. Thus, using this approach, the required forces for the object manipulation to be supplied by actuators are:

$$\tilde{\mathbf{Q}}^{(i)} = \tilde{\mathbf{Q}}_{m}^{(i)} + \tilde{\mathbf{Q}}_{f}^{(i)} + \tilde{\mathbf{Q}}_{\text{react}}^{(i)} + \tilde{\mathbf{Q}}_{\text{supp.}}^{(i)}, \tag{7}$$

where $\tilde{\mathbf{Q}}_{m}^{(i)} \in \Re^{p}$ is the control forces for end-effector motion, $\tilde{\mathbf{Q}}_{\text{react}}^{(i)} \in \Re^{p}$ is the reaction load on the end-effectors and virtually canceled the control forces for object motion or $\tilde{\mathbf{Q}}_{f}^{(i)} \in \Re^{p}$.[21] In other words, the reaction load due to the grasp of the manipulated object will be equal to the control forces applied for the object motion, considering this control strategy at each time step. Also, $\tilde{\mathbf{Q}}_{\text{supp.}}^{(i)} \in \Re^{p}$ is the suppression control forces for the flexible members. If the motion's equations of the object are stated as:

$$\mathbf{M}\ddot{\mathbf{x}} + \mathbf{F}_{w} = \mathbf{F}_{c} + \mathbf{F}_{o} + \underline{\mathbf{G}}\mathbf{F}_{e}, \tag{8}$$

where $\underline{\mathbf{G}} \in \Re^{6 \times p}$ is the grasp matrix, $\mathbf{F}_{w} \in \Re^{6}$ is the vector of nonlinear velocity terms, $\mathbf{F}_{e} \in \Re^{p}$ is the desired exerted forces from end-effectors, $\mathbf{F}_{o} \in \Re^{6}$ describes other external forces that act on the

https://doi.org/10.1017/S0263574714002392 Published online by Cambridge University Press

object and $\mathbf{F}_c \in \Re^6$ is the contact force. Choosing the Control Law for the object motion as:

$$\boldsymbol{\upsilon} = \ddot{\mathbf{x}}_d + \mathbf{K}_d(\dot{\mathbf{x}}_d - \dot{\mathbf{x}}) + \mathbf{K}_p(\mathbf{x}_d - \mathbf{x}), \tag{9}$$

where $\mathbf{e} = \mathbf{x}_d - \mathbf{x}$ is the tracking error of object variables and $\mathbf{K}_d, \mathbf{K}_p \in \Re^{6\times 6}$ are the gain matrices for the proposed controller. Then, the desired forces to move the object is obtained as:

$$\mathbf{F}_{e_{req}} = \underline{\mathbf{G}}^{\#} \left\{ \mathbf{M}\upsilon + \mathbf{F}_w - (\mathbf{F}_c + \mathbf{F}_o) \right\}, \tag{10}$$

where $\underline{\mathbf{G}}^{\#}$ is the pseudo inverse of $\underline{\mathbf{G}}$. Therefore, the desired forces to be exerted by the end-effectors so that the object is moved are obtained directly as:

$$\tilde{\mathbf{Q}}_f^{(i)} = \mathbf{F}_{e_{req}}. \tag{11}$$

Similarly, choosing the same control law for each end-effector yields:

$$\tilde{\boldsymbol{\upsilon}}^{(i)} = \ddot{\tilde{\mathbf{X}}}_d^{(i)} + \tilde{\mathbf{K}}_d \left(\dot{\tilde{\mathbf{X}}}_d^{(i)} - \dot{\tilde{\mathbf{X}}}^{(i)} \right) + \tilde{\mathbf{K}}_p(\tilde{\mathbf{X}}_d^{(i)} - \tilde{\mathbf{X}}^{(i)}), \tag{12}$$

where $\tilde{\mathbf{e}}^{(i)} = \tilde{\mathbf{X}}_d^{(i)} - \tilde{\mathbf{X}}^{(i)}$ is the system tracking error, and $\tilde{\mathbf{K}}_d, \tilde{\mathbf{K}}_p \in \Re^{p\times p}$ are positive definite (usually diagonal) gain matrices. Thus, the required force to move the end-effectors is expressed as:

$$\tilde{\mathbf{Q}}_m^{(i)} = \tilde{\mathbf{H}}^{(i)}(\mathbf{q}^{(i)})\tilde{\boldsymbol{\upsilon}}^{(i)} + \tilde{\mathbf{C}}^{(i)}(\mathbf{q}^{(i)}, \dot{\mathbf{q}}^{(i)}). \tag{13}$$

Note that $\dot{\tilde{\mathbf{X}}}_d^{(i)} \in \Re^p$ and $\tilde{\mathbf{X}}_d^{(i)} \in \Re^p$ can be obtained using the planned trajectory for the object motion and the grasp condition. To control the flexible members and to compute the suppression control force or $\tilde{\mathbf{Q}}_{supp.}^{(i)}$, the motion's equations of these members or Eq. (1) are rewritten by assuming that they are activated by some piezoelectric patches which are installed at the tip of the flexible solar panels as:[37]

$$\mathbf{M}_f^{\{i\}}\ddot{\bar{\mathbf{q}}}^{\{i\}} + \mathbf{K}^{\{i\}}\bar{\mathbf{q}}^{\{i\}} = \mathbf{Q}_e^{\{i\}} + \mathbf{Q}_v^{\{i\}} + \boldsymbol{\tau}^{\{i\}}, \tag{14}$$

where $\boldsymbol{\tau}^{\{i\}} \in \Re^m$ is the generalized actuator force which can be given by:[38]

$$\boldsymbol{\tau}^{\{i\}} = \mathbf{K}_{PZ}^{\{i\}}.\mathbf{v}_a^{\{i\}}, \tag{15}$$

where $\mathbf{K}_{PZ}^{\{i\}} \in \Re^{m\times l}$ is the mechanical coefficient of the piezoelectric actuators, which is a function of their material properties, and $\mathbf{v}_a^{\{i\}} \in \Re^l$ is the vector of voltage at each flexible member actuators. If we consider the control low of the {i}-th flexible members as:

$$\boldsymbol{\tau}^{\{i\}} = \mathbf{M}_f^{\{i\}}\ddot{\bar{\mathbf{q}}}_d^{\{i\}} + \mathbf{B}_{f_{virtual}}^{\{i\}}(\dot{\bar{\mathbf{q}}}^{\{i\}} - \dot{\bar{\mathbf{q}}}_d^{\{i\}}) + \mathbf{K}^{\{i\}}\bar{\mathbf{q}}_d^{\{i\}} - \mathbf{Q}_v^{\{i\}}, \tag{16}$$

where $\mathbf{B}_{f_{virtual}}^{\{i\}} \in \Re^{m\times m}$ is the virtual damping. This supplies a starting point for the control law to design the amount of the virtual damping. Then at last, the suppression control law for the flexible members is obtained as:

$$\tilde{\mathbf{Q}}_{supp.}^{(i)} = -\sum_{\{i\}=\{1\}}^{\{n_b\}} \mathbf{J}_c^{(i)^{-T}} \boldsymbol{\tau}^{\{i\}}, \tag{17}$$

where n_b is the number of the flexible members of the assumed robotic system. It should be noted that this force is directly applied on the flexible members using the RIFM approach which one is the advantage of this modeling approach in this model-based control algorithm. Moreover, the linear

https://doi.org/10.1017/S0263574714002392 Published online by Cambridge University Press

dynamics of the error is obtained by substituting Eqs. (17), (13) and (11) into Eq. (7), and then the result of these substitutions into Eq. (5), yielding:

$$\tilde{\mathbf{H}}^{(i)}(\mathbf{q}^{(i)})\left\{\ddot{\tilde{\mathbf{X}}}^{(i)} - \left[\ddot{\tilde{\mathbf{X}}}_d^{(i)} + \tilde{\mathbf{K}}_d(\dot{\tilde{\mathbf{X}}}_d^{(i)} - \dot{\tilde{\mathbf{X}}}^{(i)}) + \tilde{\mathbf{K}}_p(\tilde{\mathbf{X}}_d^{(i)} - \tilde{\mathbf{X}}^{(i)})\right]\right\} = \mathbf{0}$$

$$\mathbf{M}\left\{\ddot{\mathbf{x}} - \left[\ddot{\mathbf{x}}_d + \mathbf{K}_d(\dot{\mathbf{x}}_d - \dot{\mathbf{x}}) + \mathbf{K}_p(\mathbf{x}_d - \mathbf{x})\right]\right\} = \mathbf{0}. \tag{18}$$

Note that, if the flexible members are controlled by the suppression control law, then the resulting second order form of the error dynamics with zero driving terms can be used to show that the errors converge to zero asymptotically; the linear dynamic of the error of these members leads to zeros. Therefore, based on Eq. (4) $\mathbf{Q}_{\text{flex.}}(\mathbf{q}) = 0$. Indeed, considering that $\tilde{\mathbf{H}}^{(i)}$ and $\mathbf{M}$ are the positive definite matrices, Eqs. (18) result in:

$$\ddot{\tilde{\mathbf{e}}}^{(i)} + \tilde{\mathbf{K}}_d\dot{\tilde{\mathbf{e}}}^{(i)} + \tilde{\mathbf{K}}_p\tilde{\mathbf{e}}^{(i)} = \mathbf{0}$$

$$\ddot{\mathbf{e}} + \mathbf{K}_d\dot{\mathbf{e}} + \mathbf{K}_p\mathbf{e} = \mathbf{0}. \tag{19}$$

Note that the value of these gains can be obtained by trial and error and the responses comparison. Also, it has been recommended that the same controller gains should be chosen for the manipulated object and end-effectors.[21]

4. Adaptive Hybrid Suppression Control

As stated before, using a virtual damping in HSC algorithm, oscillations of the flexible members are controlled and therefore, the linear error dynamics leads to zero steady state errors. Also, to minimize disturbances of these flexible members, which act on the rigid subsystem, an adaptive law is composed with HSC. This adaptation law updates the value of the virtual damping to reduce the magnitude of the flexible member deflection at each time step. This results in a perfect tracking for the system variables during an object manipulation task. In fact, in order to achieve a better performance, the error dynamics of the flexible subsystem should be finely controlled, while it is desired to determine an appropriate value for the virtual damping.[13] This value is obtained to guarantee that the roots of characteristics equation for the linearized error dynamics of the flexible subsystem are placed on the left complex plane. Therefore, finding this appropriate value for the virtual damping is the key strategy to solve the problem of fast dynamics in such systems. This adaptation rule certainly takes into account the saturation limits of the actuators during the task.

It is assumed that $\mathbf{B}_{f_{virtual}}^{\{i\}}$ is a desired value for the virtual damping which should be obtained using an adaptation law, then the control law of each flexible body or Eq. (16) can be modified as:

$$\boldsymbol{\tau}^{\{i\}} = \mathbf{M}_f^{\{i\}}\ddot{\bar{\mathbf{q}}}_d^{\{i\}} + \hat{\mathbf{B}}_{f_{virtual}}^{\{i\}}(\dot{\bar{\mathbf{q}}}_d^{\{i\}} - \dot{\bar{\mathbf{q}}}^{\{i\}}) + \mathbf{K}^{\{i\}}\bar{\mathbf{q}}_d^{\{i\}} - \mathbf{Q}_v^{\{i\}}, \tag{20}$$

where $\hat{\mathbf{B}}_{f_{virtual}}^{\{i\}}$ is an estimated value for $\mathbf{B}_{f_{virtual}}^{\{i\}}$ that is calculated at each time step and substituted into the control law. Therefore, the closed loop dynamics of error of each flexible body can be written as:

$$\mathbf{M}_f^{\{i\}}\ddot{\mathbf{e}}_f^{\{i\}} + \hat{\mathbf{B}}_{f_{virtual}}^{\{i\}}\dot{\mathbf{e}}_f^{\{i\}} + \mathbf{K}^{\{i\}}\mathbf{e}_f^{\{i\}} = \mathbf{Q}_e^{\{i\}}, \tag{21}$$

where $\mathbf{e}_f^{\{i\}} = \bar{\mathbf{q}}_d^{\{i\}} - \bar{\mathbf{q}}^{\{i\}}$. Since, it was assumed that $\mathbf{B}_{f_{virtual}}^{\{i\}}$ is the desired value of virtual damping and $\hat{\mathbf{B}}_{f_{virtual}}^{\{i\}}$ is its estimated value, so $\tilde{\mathbf{B}}_{f_{virtual}}^{\{i\}}$ is defined as the corresponding estimation error:

$$\tilde{\mathbf{B}}_{f_{virtual}}^{\{i\}} = \mathbf{B}_{f_{virtual}}^{\{i\}} - \hat{\mathbf{B}}_{f_{virtual}}^{\{i\}}. \tag{22}$$

https://doi.org/10.1017/S0263574714002392 Published online by Cambridge University Press

Substituting Eq. (22) into (21) and after some simplifications, the following error equation is obtained:

$$\ddot{\mathbf{e}}_{\mathrm{f}}^{\{\mathrm{i}\}} + (\mathbf{M}_{\mathrm{f}}^{\{\mathrm{i}\}})^{-1}\mathbf{B}_{\mathrm{f_{virtual}}}^{\{\mathrm{i}\}}\dot{\mathbf{e}}_{\mathrm{f}}^{\{\mathrm{i}\}} + (\mathbf{M}_{\mathrm{f}}^{\{\mathrm{i}\}})^{-1}\mathbf{K}^{\{\mathrm{i}\}}\mathbf{e}_{\mathrm{f}}^{\{\mathrm{i}\}} = (\mathbf{M}_{\mathrm{f}}^{\{\mathrm{i}\}})^{-1}\left\{\mathbf{Q}_{\mathrm{e}}^{\{\mathrm{i}\}} + \tilde{\mathbf{B}}_{\mathrm{f_{virtual}}}^{\{\mathrm{i}\}}\dot{\mathbf{e}}_{\mathrm{f}}^{\{\mathrm{i}\}}\right\} \tag{23}$$

or equivalently:

$$\ddot{\mathbf{e}}_{\mathrm{f}}^{\{\mathrm{i}\}} + (\mathbf{M}_{\mathrm{f}}^{\{\mathrm{i}\}})^{-1}\mathbf{B}_{\mathrm{f_{virtual}}}^{\{\mathrm{i}\}}\dot{\mathbf{e}}_{\mathrm{f}}^{\{\mathrm{i}\}} + (\mathbf{M}_{\mathrm{f}}^{\{\mathrm{i}\}})^{-1}\mathbf{K}^{\{\mathrm{i}\}}\mathbf{e}_{\mathrm{f}}^{\{\mathrm{i}\}} = (\mathbf{M}_{\mathrm{f}}^{\{\mathrm{i}\}})^{-1}\underline{\mathbf{K}}(\bar{\mathbf{q}}, \dot{\bar{\mathbf{q}}}, \ddot{\bar{\mathbf{q}}})\tilde{\mathbf{B}}_{\mathrm{f_{virtual}}}^{\{\mathrm{i}\}}, \tag{24}$$

where $\underline{\mathbf{K}} \in \Re^{\mathrm{m}\times\mathrm{m}}$ is defined as the regressor matrix. Thus, the error dynamics for each flexible body are obtained in the state space form as:

$$\dot{\underline{\mathbf{X}}} = \underline{\mathbf{A}}\underline{\mathbf{X}} + \underline{\mathbf{B}}\left[(\mathbf{M}_{\mathrm{f}}^{\{\mathrm{i}\}})^{-1}\underline{\mathbf{K}}\tilde{\mathbf{B}}_{\mathrm{f_{virtual}}}^{\{\mathrm{i}\}}\right]$$

$$\underline{\mathbf{Y}} = \underline{\mathbf{C}}\underline{\mathbf{X}}, \tag{25}$$

where $\underline{\mathbf{Y}} \in \Re^{2\mathrm{m}}$ is the filtered output and $\underline{\mathbf{X}} \in \Re^{2\mathrm{m}}$ is:

$$\underline{\mathbf{X}} = \begin{Bmatrix} \mathrm{e}_{\mathrm{f_1}}^{\{\mathrm{i}\}} \\ \dot{\mathrm{e}}_{\mathrm{f_1}}^{\{\mathrm{i}\}} \\ \vdots \end{Bmatrix}_{2\mathrm{m}} \tag{26}$$

and $\underline{\mathbf{A}} \in \Re^{2\mathrm{m}\times2\mathrm{m}}$, $\underline{\mathbf{B}} \in \Re^{2\mathrm{m}\times\mathrm{m}}$ and $\underline{\mathbf{C}} \in \Re^{\mathrm{m}\times2\mathrm{m}}$ matrices are defined by:

$$\underline{\mathbf{A}} = \begin{bmatrix} \mathbf{0} & \mathbf{I} \\ -(\mathbf{M}_{\mathrm{f}}^{\{\mathrm{i}\}})^{-1}\underline{\mathbf{K}} & -(\mathbf{M}_{\mathrm{f}}^{\{\mathrm{i}\}})^{-1}\tilde{\mathbf{B}}_{\mathrm{f_{virtual}}}^{\{\mathrm{i}\}} \end{bmatrix}, \quad \underline{\mathbf{B}} = \begin{bmatrix} \mathbf{0} \\ \mathbf{I} \end{bmatrix}, \quad \underline{\mathbf{C}} = \begin{bmatrix} \mathbf{I} & \mathbf{0} \end{bmatrix}. \tag{27}$$

Next, to obtain the adaptation law required to calculate and update the virtual damping amount as well as to ensure system stability, we define a Lyapunov function. This function is given by:

$$\mathbf{V}(\mathbf{e}_{\mathrm{f}}, \dot{\mathbf{e}}_{\mathrm{f}}) = \underline{\mathbf{X}}^{\mathrm{T}}\underline{\rho}\underline{X} + \tilde{\mathbf{B}}_{\mathrm{f_{virtual}}}^{\{\mathrm{i}\}}\Gamma^{-1}\tilde{\mathbf{B}}_{\mathrm{f_{virtual}}}^{\{\mathrm{i}\}^{\mathrm{T}}}, \tag{28}$$

where $\Gamma = \mathrm{diag}[\,\gamma_1\ \gamma_2\ \ldots\ \gamma_{\mathrm{r}}\,]_{\mathrm{m}\times\mathrm{m}}$, $\gamma_{\mathrm{i}} > 0$ is the gain matrix. Considering the Kalman–Yakubovich–Popov lemma,[39] if the system is stable, then there exist symmetric and positive definite $\underline{\boldsymbol{\rho}} \in \Re^{2\mathrm{m}\times2\mathrm{m}}$ and $\underline{\mathbf{Q}} \in \Re^{2\mathrm{m}\times2\mathrm{m}}$ matrices which satisfy the following equations as:

$$\underline{\mathbf{A}}^{\mathrm{T}}\underline{\boldsymbol{\rho}} + \underline{\boldsymbol{\rho}}\underline{\mathbf{A}} = -\underline{\mathbf{Q}}$$

$$\underline{\boldsymbol{\rho}}\underline{\mathbf{B}} = \underline{\mathbf{C}}^{\mathrm{T}} \rightarrow \underline{\mathbf{B}}^{\mathrm{T}}\underline{\boldsymbol{\rho}}^{\mathrm{T}} = \underline{\mathbf{C}} \rightarrow \underline{\mathbf{B}}^{\mathrm{T}}\underline{\boldsymbol{\rho}} = \underline{\mathbf{C}}. \tag{29}$$

Considering that Lyapunov function given by Eq. (28) is positive definite, we study the derivative of this function:

$$\dot{\mathbf{V}}(\mathbf{e}_{\mathrm{f}}, \dot{\mathbf{e}}_{\mathrm{f}}) = \dot{\underline{\mathbf{X}}}^{\mathrm{T}}\underline{\boldsymbol{\rho}}\underline{X} + \underline{\mathbf{X}}^{\mathrm{T}}\underline{\boldsymbol{\rho}}\dot{\underline{X}} + 2\tilde{\mathbf{B}}_{\mathrm{f_{virtual}}}^{\{\mathrm{i}\}^{\mathrm{T}}}\Gamma^{-1}\dot{\tilde{\mathbf{B}}}_{\mathrm{f_{virtual}}}^{\{\mathrm{i}\}}. \tag{30}$$

Substituting form Eq. (25) into this equation yields:

$$\dot{\mathbf{V}}(\mathbf{e}_{\mathrm{f}}, \dot{\mathbf{e}}_{\mathrm{f}}) = \left[\underline{\mathbf{A}}\underline{\mathbf{X}} + \underline{\mathbf{B}}((\mathbf{M}_{\mathrm{f}}^{\{\mathrm{i}\}})^{-1}\underline{\mathbf{K}}\tilde{\mathbf{B}}_{\mathrm{f_{virtual}}}^{\{\mathrm{i}\}})\right]^{\mathrm{T}}\underline{\boldsymbol{\rho}}\underline{X} + \underline{\mathbf{X}}^{\mathrm{T}}\underline{\boldsymbol{\rho}}\left[\underline{\mathbf{A}}\underline{\mathbf{X}} + \underline{\mathbf{B}}((\mathbf{M}_{\mathrm{f}}^{\{\mathrm{i}\}})^{-1}\underline{\mathbf{K}}\tilde{\mathbf{B}}_{\mathrm{f_{virtual}}}^{\{\mathrm{i}\}})\right]$$
$$+ 2\tilde{\mathbf{B}}_{\mathrm{f_{virtual}}}^{\{\mathrm{i}\}^{\mathrm{T}}}\Gamma^{-1}\dot{\tilde{\mathbf{B}}}_{\mathrm{f_{virtual}}}^{\{\mathrm{i}\}} \tag{31}$$

https://doi.org/10.1017/S0263574714002392 Published online by Cambridge University Press

which can be rearranged as:

$$\dot{\mathbf{V}}(\mathbf{e}_\mathrm{f}, \dot{\mathbf{e}}_\mathrm{f}) = \underline{\mathbf{X}}^\mathrm{T}\underline{\mathbf{A}}^\mathrm{T}\underline{\rho}\underline{X} + \underline{\mathbf{X}}^\mathrm{T}\underline{\rho}\underline{\mathbf{A}}\underline{\mathbf{X}} + 2\tilde{\mathbf{B}}_{\mathrm{f}_{\mathrm{virtual}}}^{\{\mathrm{i}\}^\mathrm{T}}\Gamma^{-1}\dot{\tilde{\mathbf{B}}}_{\mathrm{f}_{\mathrm{virtual}}}^{\{\mathrm{i}\}} + \left[\underline{\mathbf{B}}(\mathbf{M}_\mathrm{f}^{\{\mathrm{i}\}})^{-1}\underline{\mathbf{K}}\tilde{\mathbf{B}}_{\mathrm{f}_{\mathrm{virtual}}}^{\{\mathrm{i}\}}\right]^\mathrm{T}\underline{\rho}\underline{X} + \underline{\mathbf{X}}^\mathrm{T}\underline{\rho}\underline{\mathbf{B}}(\mathbf{M}_\mathrm{f}^{\{\mathrm{i}\}})^{-1}\underline{\mathbf{K}}\tilde{\mathbf{B}}_{\mathrm{f}_{\mathrm{virtual}}}^{\{\mathrm{i}\}}. \tag{32}$$

After some simplifications and considering the fact that $((\mathbf{M}_\mathrm{f}^{\{\mathrm{i}\}})^{-1})^\mathrm{T} = (\mathbf{M}_\mathrm{f}^{\{\mathrm{i}\}})^{-1}$, we can rewrite this equation as:

$$\dot{\mathbf{V}}(\mathbf{e}_\mathrm{f}, \dot{\mathbf{e}}_\mathrm{f}) = \underline{\mathbf{X}}^\mathrm{T}\left[\underline{\mathbf{A}}^\mathrm{T}\underline{\rho} + \underline{\rho}\underline{\mathbf{A}}\right]\underline{\mathbf{X}} + 2\tilde{\mathbf{B}}_{\mathrm{f}_{\mathrm{virtual}}}^{\{\mathrm{i}\}^\mathrm{T}}\Gamma^{-1}\dot{\tilde{\mathbf{B}}}_{\mathrm{f}_{\mathrm{virtual}}}^{\{\mathrm{i}\}} + \tilde{\mathbf{B}}_{\mathrm{f}_{\mathrm{virtual}}}^{\{\mathrm{i}\}^\mathrm{T}}\underline{\mathbf{K}}^\mathrm{T}(\mathbf{M}_\mathrm{f}^{\{\mathrm{i}\}})^{-1}\underline{\mathbf{B}}^\mathrm{T}\underline{\rho}\underline{\mathbf{X}} + \tilde{\mathbf{B}}_{\mathrm{f}_{\mathrm{virtual}}}^{\{\mathrm{i}\}^\mathrm{T}}\underline{\mathbf{K}}^\mathrm{T}(\mathbf{M}_\mathrm{f}^{\{\mathrm{i}\}})^{-1}\underline{\mathbf{B}}^\mathrm{T}\underline{\rho}\underline{\mathbf{X}}. \tag{33}$$

Thus

$$\dot{\mathbf{V}}(\mathbf{e}_\mathrm{f}, \dot{\mathbf{e}}_\mathrm{f}) = -\underline{\mathbf{X}}^\mathrm{T}\underline{\mathbf{Q}}\underline{\mathbf{X}} + 2\tilde{\mathbf{B}}_{\mathrm{f}_{\mathrm{virtual}}}^{\{\mathrm{i}\}^\mathrm{T}}\left[\Gamma^{-1}\dot{\tilde{\mathbf{B}}}_{\mathrm{f}_{\mathrm{virtual}}}^{\{\mathrm{i}\}} + \underline{\mathbf{K}}^\mathrm{T}(\mathbf{M}_\mathrm{f}^{\{\mathrm{i}\}})^{-1}\underline{\mathbf{B}}^\mathrm{T}\underline{\rho}\underline{\mathbf{X}}\right]. \tag{34}$$

Using Eq. (25), it is concluded that:

$$\dot{\mathbf{V}}(\mathbf{e}_\mathrm{f}, \dot{\mathbf{e}}_\mathrm{f}) = -\underline{\mathbf{X}}^\mathrm{T}\underline{\mathbf{Q}}\underline{\mathbf{X}} + 2\tilde{\mathbf{B}}_{\mathrm{f}_{\mathrm{virtual}}}^{\{\mathrm{i}\}^\mathrm{T}}\left[\Gamma^{-1}\dot{\tilde{\mathbf{B}}}_{\mathrm{f}_{\mathrm{virtual}}}^{\{\mathrm{i}\}} + \underline{\mathbf{K}}^\mathrm{T}(\mathbf{M}_\mathrm{f}^{\{\mathrm{i}\}})^{-1}\underline{\mathbf{C}}\underline{\mathbf{X}}\right] \tag{35}$$

or:

$$\dot{\mathbf{V}}(\mathbf{e}_\mathrm{f}, \dot{\mathbf{e}}_\mathrm{f}) = -\underline{\mathbf{X}}^\mathrm{T}\underline{\mathbf{Q}}\underline{\mathbf{X}} + 2\tilde{\mathbf{B}}_{\mathrm{f}_{\mathrm{virtual}}}^{\{\mathrm{i}\}^\mathrm{T}}\left[\Gamma^{-1}\dot{\tilde{\mathbf{B}}}_{\mathrm{f}_{\mathrm{virtual}}}^{\{\mathrm{i}\}} + \underline{\mathbf{K}}^\mathrm{T}(\mathbf{M}_\mathrm{f}^{\{\mathrm{i}\}})^{-1}\underline{\mathbf{Y}}\right]. \tag{36}$$

Since, the first term in the right hand side of the above equation is always negative (not semi-negative, because $\underline{\mathbf{Q}}$ is defined as a positive matrix), if the second term of this equation becomes equal to zero, then derivative of Lyapunov function becomes negative definite, $\dot{\mathbf{V}}(\mathbf{e}_\mathrm{f}, \dot{\mathbf{e}}_\mathrm{f}) < \mathbf{0}$, and thus the system is stable. Therefore, we choose:

$$\dot{\tilde{\mathbf{B}}}_{\mathrm{f}_{\mathrm{virtual}}}^{\{\mathrm{i}\}} = -\Gamma\underline{\mathbf{K}}^\mathrm{T}(\mathbf{M}_\mathrm{f}^{\{\mathrm{i}\}})^{-1}\underline{\mathbf{Y}}, \tag{37}$$

where according to the definition of estimated parameters we have:

$$\tilde{\mathbf{B}}_{\mathrm{f}_{\mathrm{virtual}}}^{\{\mathrm{i}\}} = \mathbf{B}_{\mathrm{f}_{\mathrm{virtual}}}^{\{\mathrm{i}\}} - \hat{\mathbf{B}}_{\mathrm{f}_{\mathrm{virtual}}}^{\{\mathrm{i}\}} \rightarrow \dot{\tilde{\mathbf{B}}}_{\mathrm{f}_{\mathrm{virtual}}}^{\{\mathrm{i}\}} = -\dot{\hat{\mathbf{B}}}_{\mathrm{f}_{\mathrm{virtual}}}^{\{\mathrm{i}\}} \tag{38}$$

and the adaptation law is obtained from Lyapunov method for unknown parameters of the system as:

$$\dot{\hat{\mathbf{B}}}_{\mathrm{f}_{\mathrm{virtual}}}^{\{\mathrm{i}\}} = \Gamma\underline{\mathbf{K}}^\mathrm{T}(\mathbf{M}_\mathrm{f}^{\{\mathrm{i}\}})^{-1}\underline{\mathbf{Y}}. \tag{39}$$

A block diagram of the implementation procedure of this control algorithm for cooperative object manipulation is shown in Fig. 2. The performance improvement of the AHSC compared to the HSC is studied next.

5. Case Study

SFFRs are space robotic systems equipped with a single or multiple manipulators and thrusters jets on a flying base (satellite). These thrusters were originally proposed as on-off cold jets, while recently hot continuous ones have been introduced. Distinct from fixed-based manipulators, the base of a SFFR responds to dynamic reaction forces due to the arms motion. Unlike long reach space manipulators, SFFR are suggested to be comparable to the size of an astronaut, and are usually investigated under the

https://doi.org/10.1017/S0263574714002392 Published online by Cambridge University Press

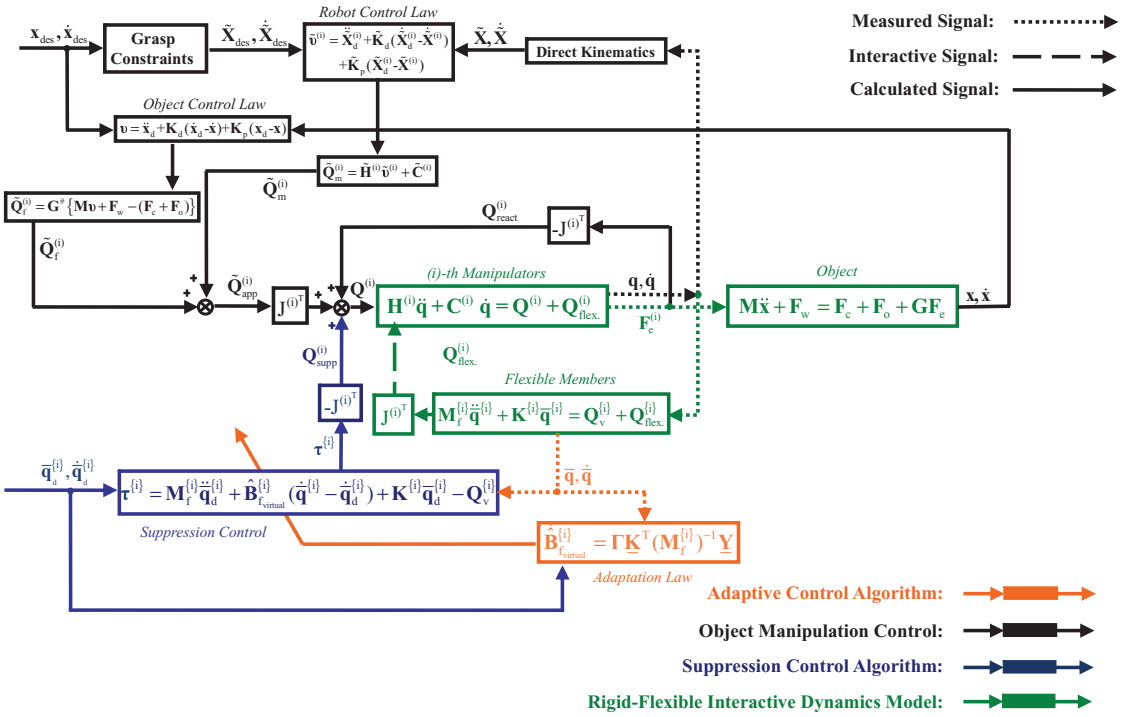

Fig. 2. Block diagram of RFIM and AHSC algorithm for cooperative object manipulation.

assumption of rigid elements. Here, the considered SFFR system contains a main rigid body equipped with two manipulating arms and two flexible solar panels. The system also includes a rotating antenna and a photo capturing camera as its third and fourth arm. As mentioned before, the exploited RFIM approach may be interpreted as a method that combines the Lagrange and Newton–Euler methods. So, the coupling between the rigid subsystem and the flexible one is restricted to the constraint forces which are computed at each time step, and applied to the rigid part for computations of the next time step. This compact model of the rigid–flexible multi-body systems can be used to study the dynamics effects of flexible members. Also, in applying model-based control algorithm such as the proposed AHSC for cooperative object manipulation control, this compact model is highly useful, as discussed below.

5.1. Dynamics modeling of SFFR

The closed-form dynamics equations of a SFFR with just rigid components were obtained and verified.[40] Considering the flexible appendages with the specifications described,[41] the dynamics model of the rigid SFFR of Fig. 3 is modified and expressed as:[25]

$$\mathbf{H}(\boldsymbol{\beta_0}, \boldsymbol{\theta})\,\ddot{\mathbf{q}} + \mathbf{C_1}(\boldsymbol{\beta_0}, \dot{\boldsymbol{\beta}}_\mathbf{0}, \boldsymbol{\theta}, \dot{\boldsymbol{\theta}})\,\dot{\mathbf{q}} + \mathbf{C_2}(\boldsymbol{\beta_0}, \dot{\boldsymbol{\beta}}_\mathbf{0}, \boldsymbol{\theta}, \dot{\boldsymbol{\theta}}) = \mathbf{Q}(\boldsymbol{\beta_0}, \boldsymbol{\theta}) + \mathbf{Q}_{\text{flex.}}(\boldsymbol{\beta_0}), \tag{40}$$

where $\mathbf{Q}_{\text{flex.}}(\beta_\mathbf{0})$ is the generalized resultant forces/torques applied on the main body of the SFFR due to vibrating motion of the flexible solar panels, and

$$\begin{aligned}\mathbf{H}_{ij} = {} & \mathrm{M}_{sys}\frac{\partial \mathbf{R}_{C_0}}{\partial q_i}\cdot\frac{\partial \mathbf{R}_{C_0}}{\partial q_j} + \frac{{}^0\partial\omega_0}{\partial \dot{q}_i}\cdot\mathbf{I}_0\cdot\frac{{}^0\partial\omega_0}{\partial \dot{q}_j} \\ & + \sum_{m=1}^{n}\sum_{k=1}^{N_m}\left(m_k^{(m)}\frac{\partial \mathbf{r}_{C_k}^{(m)}}{\partial q_i}\cdot\frac{\partial \mathbf{r}_{C_k}^{(m)}}{\partial q_j} + \frac{{}^k\partial\omega_k^{(m)}}{\partial \dot{q}_i}\cdot\mathbf{I}_k^{(m)}\cdot\frac{{}^k\partial\omega_k^{(m)}}{\partial \dot{q}_j}\right) \\ & + \left(\sum_{m=1}^{n}\sum_{k=1}^{N_m}m_k^{(m)}\frac{\partial \mathbf{r}_{C_k}^{(m)}}{\partial q_i}\right)\cdot\frac{\partial \mathbf{R}_{C_0}}{\partial q_j} + \left(\sum_{m=1}^{n}\sum_{k=1}^{N_m}m_k^{(m)}\frac{\partial \mathbf{r}_{C_k}^{(m)}}{\partial q_j}\right)\cdot\frac{\partial \mathbf{R}_{C_0}}{\partial q_i}\end{aligned} \tag{41a}$$

https://doi.org/10.1017/S0263574714002392 Published online by Cambridge University Press

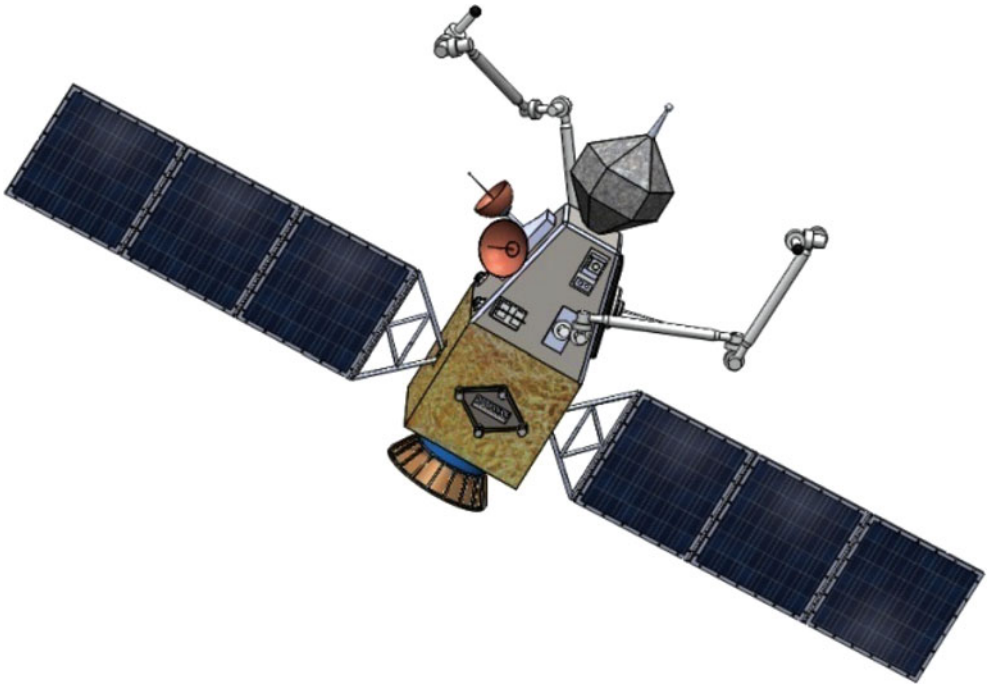

Fig. 3. The considered space robotic system which includes two flexible solar panels.

$$\mathbf{C}_{1ij} = \mathrm{M}_{sys}\frac{\partial \mathbf{R}_{C_0}}{\partial \mathrm{q_i}} \cdot \left(\sum_{s=1}^{N}\frac{\partial^2 \mathbf{R}_{C_0}}{\partial \mathrm{q_s}\partial \mathrm{q_j}}\dot{\mathrm{q}}_s\right) + \frac{{}^0\partial\omega_0}{\partial \dot{\mathrm{q}}_i}\mathbf{I}_0\frac{{}^0\partial\omega_0}{\partial \mathrm{q_j}} + \omega_0\mathbf{I}_0\frac{{}^0\partial^2\omega_0}{\partial \dot{\mathrm{q}}_i\partial \mathrm{q_j}}$$
$$+ \sum_{m=1}^{n}\sum_{k=1}^{N_m}\left(\mathrm{m}_k^{(m)}\frac{\partial \mathbf{r}_{C_k}^{(m)}}{\partial \mathrm{q_i}} \cdot \left(\sum_{s=1}^{N}\frac{\partial^2 \mathbf{r}_{C_k}^{(m)}}{\partial \mathrm{q_s}\partial \mathrm{q_j}}\dot{\mathrm{q}}_s\right) + \frac{{}^k\partial\omega_k^{(m)}}{\partial \dot{\mathrm{q}}_i}\mathbf{I}_k^{(m)}\frac{{}^k\partial\omega_k^{(m)}}{\partial \mathrm{q_j}} + \omega_k^{(m)}\mathbf{I}_k^{(m)}\frac{{}^k\partial^2\omega_k^{(m)}}{\partial \dot{\mathrm{q}}_i\partial \mathrm{q_j}}\right)$$
$$+ \left(\sum_{s=1}^{N}\frac{\partial^2 \mathbf{R}_{C_0}}{\partial \mathrm{q_s}\partial \mathrm{q_i}}\dot{\mathrm{q}}_s\right) \cdot \sum_{m=1}^{n}\sum_{k=1}^{N_m}\left(\mathrm{m}_k^{(m)}\frac{\partial \mathbf{r}_{C_k}^{(m)}}{\partial \mathrm{q_j}}\right) + \frac{\partial \mathbf{R}_{C_0}}{\partial \mathrm{q_i}} \cdot \sum_{m=1}^{n}\sum_{k=1}^{N_m}\left(\mathrm{m}_k^{(m)}\sum_{s=1}^{N}\frac{\partial^2 \mathbf{r}_{C_k}^{(m)}}{\partial \mathrm{q_s}\partial \mathrm{q_j}}\dot{\mathrm{q}}_s\right) \quad (41b)$$

$$\mathbf{C}_{2i} = -\left(\omega_0\mathbf{I}_0\frac{{}^0\partial\omega_0}{\partial \mathrm{q_i}} + \sum_{m=1}^{n}\sum_{k=1}^{N_m}\omega_k^{(m)}\mathbf{I}_k^{(m)}\frac{{}^k\partial\omega_k^{(m)}}{\partial \mathrm{q_i}}\right), \quad (41c)$$

where ω_0 and $\mathbf{I}_0$ are angular velocity vector and moment of inertia matrix of the base, M_{sys} is the total mass of the rigid subsystem, $\omega_k^{(m)}$ is the angular velocity of the k-th link of the (m)-th manipulator, $\mathbf{r}_{C_k}^{(m)}$ is the position vector of mass center of this link, $\mathrm{m}_k^{(m)}$ its mass, and $\mathbf{I}_k^{(m)}$ its inertia matrix, and $\mathbf{R}_{C_0}$ is the inertial position vector of mass center of the base. The column vector $\mathbf{q}$ describes the rigid subsystem generalized variables defined as:

$$\mathbf{q} = \left\{\mathbf{R}_{C_0}^{T}, \quad \boldsymbol{\beta}_0^{T}, \quad \boldsymbol{\theta}^{T}\right\}^{T}, \quad (42)$$

where β_0 is a set of Euler angles that determines the orientation of the base, and θ describes joint angle of the links that is defined as:

$$\theta^{T} = \left\{\theta_1^{(1)},\ldots,\theta_{N_1}^{(1)},\ldots,\theta_1^{(m)},\ldots,\theta_{N_m}^{(m)},\ldots,\theta_1^{(n)},\ldots,\theta_{N_n}^{(n)}\right\}^{T}, \quad (43)$$

https://doi.org/10.1017/S0263574714002392 Published online by Cambridge University Press

where n is the number of manipulators, N_m is the number of links of the (m)-th manipulator, and $\theta_i^{(m)}$ describes the corresponding joint angles of the m-th of manipulator. Also, **Q** describes the vector of generalized forces and torques.[41] Thus, Eq. (40) presents the equations of motion of a rigid SFFR in space, considered to be a microgravity environment. Next, using the introduced RFIM approach for system modeling, the solar panels of the SFFR can be considered as a flexible beam in planar deformations. The main problem in this modeling is to select the appropriate displacement field or the shape functions for flexible bodies. Therefore, assuming a fixed end beam for the panel, we can choose a displacement field as below:

$$\mathbf{S}^{\{i\}} = \begin{bmatrix} \xi & 0 & 0 \\ 0 & 3\xi^2 - 2\xi^3 & L_b(\xi^3 - \xi^2) \end{bmatrix}, \tag{44}$$

where ξ is a dimensionless variable defined as $\xi = x/L_b$ and L_b is the length of beam. Then, $\mathbf{L}^{\{i\}}$ matrix for absolute velocity of the flexible beam is obtained, that leads to computation of the mass matrix for flexible members, i.e. the left and right solar panels, as:

$$\mathbf{M}_f^{\{i\}} = \begin{bmatrix} m^{\{i\}} & 0 & -\frac{m^{\{i\}}}{12}(6(L_b+\bar{q}_{f_4}^{\{i\}})S\delta_0^{\{i\}}+(6\bar{q}_{f_5}^{\{i\}} - L_b\bar{q}_{f_6}^{\{i\}})C\delta_0^{\{i\}}) & \frac{m^{\{i\}}}{2}C\delta_0^{\{i\}} & -\frac{m^{\{i\}}}{2}S\delta_0^{\{i\}} & \frac{m^{\{i\}}L_b}{12}S\delta_0^{\{i\}} \\ & m^{\{i\}} & \frac{m^{\{i\}}}{12}(6(L_b+\bar{q}_{f_4}^{\{i\}})C\delta_0^{\{i\}} - (6\bar{q}_{f_5}^{\{i\}} - L_b\bar{q}_{f_6}^{\{i\}})S\delta_0^{\{i\}}) & \frac{m^{\{i\}}}{2}S\delta_0^{\{i\}} & \frac{m^{\{i\}}}{2}C\delta_0^{\{i\}} & -\frac{m^{\{i\}}L_b}{12}C\delta_0^{\{i\}} \\ & & m^{\{i\}}\left(\frac{L_b^2}{3}+\frac{2}{3}L_b\bar{q}_{f_4}^{\{i\}}+\frac{1}{3}(\bar{q}_{f_4}^{\{i\}})^2+\frac{13}{35}(\bar{q}_{f_5}^{\{i\}})^2 + \frac{L_b^2}{105}(\bar{q}_{f_6}^{\{i\}})^2 - \frac{11}{105}L_b\bar{q}_{f_5}^{i}\bar{q}_{f_6}^{\{i\}}\right) & \frac{m^{\{i\}}}{20}(-7\bar{q}_{f_5}^{\{i\}}+L_b\bar{q}_{f_6}^{\{i\}}) & \frac{m^{\{i\}}}{20}(7L_b+7\bar{q}_{f_4}^{\{i\}}) & -\frac{m^{\{i\}}}{20}(L_b^2+L_b\bar{q}_{f_4}^{\{i\}}) \\ & & & \frac{1}{3}m^{\{i\}} & 0 & 0 \\ & & & & \frac{13}{35}m^{\{i\}} & -\frac{11}{210}m^{\{i\}}L_b \\ & & \text{Symmetric} & & & \frac{m^{\{i\}}L_b^2}{105} \end{bmatrix}, \tag{45}$$

where $\bar{q}_{f_4}^{\{i\}}, \bar{q}_{f_5}^{\{i\}}, \bar{q}_{f_6}^{\{i\}}$ are the vector components of elastic coordinates of the flexible body {i}, $C\delta_0^{\{i\}}$ stands for $\cos\delta_0^{\{i\}}$, and correspondingly $S\delta_0^{\{i\}}$ for $\sin\delta_0^{\{i\}}$. As shown in Fig. 3 we have:

$$\begin{aligned} \{i\} = \{1\} \text{ or } \{L\} \text{ (Left Solar Panel)} \ &\rightarrow \ \delta_0^{\{L\}} = \beta_0 + \pi/2 \\ \{i\} = \{2\} \text{ or } \{R\} \text{ (Right Solar Panel)} &\rightarrow \delta_0^{\{R\}} = \beta_0 - \pi/2, \end{aligned} \tag{46}$$

where β_0 is the yaw angle of the base. Then, assuming that shear deformations are negligible, based on Euler–Bernoulli beam theory, the stiffness matrix is obtained as:

$$\mathbf{k}_{ff}^{\{i\}} = \begin{bmatrix} \frac{Ea}{L_b} & 0 & 0 \\ 0 & \frac{12EI}{L_b^3} & -\frac{6EI}{L_b^2} \\ 0 & -\frac{6EI}{L_b^2} & \frac{4EI}{L_b} \end{bmatrix}, \tag{47}$$

where E is the coefficient of elasticity, I is the second moment of area for the flexible solar panels, and "a" is the cross sectional of the beam. Also, the vector of quadratic velocity terms which results

https://doi.org/10.1017/S0263574714002392 Published online by Cambridge University Press

from differentiating the kinetic energy with respect to the body coordinates and time is obtained as:

$$\mathbf{Q}_{\mathrm{v}}^{\{\mathrm{i}\}}=\left\{\begin{array}{c}\frac{\mathrm{m}^{\{\mathrm{i}\}}\dot{\delta}_0^2}{12}[6(\mathrm{L_b}+\bar{\mathrm{q}}_{\mathrm{f_4}}^{\{\mathrm{i}\}})\mathrm{C}\delta_0^{\{\mathrm{i}\}}-(6\bar{\mathrm{q}}_{\mathrm{f_5}}^{\{\mathrm{i}\}}-\mathrm{L_b}\bar{\mathrm{q}}_{\mathrm{f_6}}^{\{\mathrm{i}\}})\mathrm{S}\delta_0^{\{\mathrm{i}\}}]+\frac{\mathrm{m}^{\{\mathrm{i}\}}\dot{\delta}_0}{6}[6\dot{\bar{\mathrm{q}}}_{\mathrm{f_4}}^{\{\mathrm{i}\}}\mathrm{S}\delta_0^{\{\mathrm{i}\}}+(6\dot{\bar{\mathrm{q}}}_{\mathrm{f_5}}^{\{\mathrm{i}\}}-\mathrm{L_b}\dot{\bar{\mathrm{q}}}_{\mathrm{f_6}}^{\{\mathrm{i}\}})\mathrm{C}\delta_0^{\{\mathrm{i}\}}]\\ \frac{\mathrm{m}^{\{\mathrm{i}\}}\dot{\delta}_0^2}{12}[6(\mathrm{L_b}+\bar{\mathrm{q}}_{\mathrm{f_4}}^{\{\mathrm{i}\}})\mathrm{S}\delta_0^{\{\mathrm{i}\}}+(6\bar{\mathrm{q}}_{\mathrm{f_5}}^{\{\mathrm{i}\}}-\mathrm{L_b}\bar{\mathrm{q}}_{\mathrm{f_6}}^{\{\mathrm{i}\}})\mathrm{C}\delta_0^{\{\mathrm{i}\}}]+\frac{\mathrm{m}^{\{\mathrm{i}\}}\dot{\delta}_0}{6}[-6\dot{\bar{\mathrm{q}}}_{\mathrm{f_4}}^{\{\mathrm{i}\}}\mathrm{C}\delta_0^{\{\mathrm{i}\}}+(6\dot{\bar{\mathrm{q}}}_{\mathrm{f_5}}^{\{\mathrm{i}\}}-\mathrm{L_b}\dot{\bar{\mathrm{q}}}_{\mathrm{f_6}}^{\{\mathrm{i}\}})\mathrm{S}\delta_0^{\{\mathrm{i}\}}]\\ -2\mathrm{m}^{\{\mathrm{i}\}}\dot{\delta}_0[\frac{1}{3}\dot{\bar{\mathrm{q}}}_{\mathrm{f_4}}^{\{\mathrm{i}\}}+\frac{1}{3}\dot{\bar{\mathrm{q}}}_{\mathrm{f_4}}^{\{\mathrm{i}\}}\bar{\mathrm{q}}_{\mathrm{f_4}}^{\{\mathrm{i}\}}+\frac{13}{35}\dot{\bar{\mathrm{q}}}_{\mathrm{f_5}}^{\{\mathrm{i}\}}\bar{\mathrm{q}}_{\mathrm{f_5}}^{\{\mathrm{i}\}}-\frac{11}{210}\mathrm{L_b}\dot{\bar{\mathrm{q}}}_{\mathrm{f_6}}^{\{\mathrm{i}\}}\bar{\mathrm{q}}_{\mathrm{f_5}}^{\{\mathrm{i}\}}-\frac{11}{210}\mathrm{L_b}\dot{\bar{\mathrm{q}}}_{\mathrm{f_5}}^{\{\mathrm{i}\}}\bar{\mathrm{q}}_{\mathrm{f_6}}^{\{\mathrm{i}\}}+\frac{\mathrm{L_b^2}}{105}\dot{\bar{\mathrm{q}}}_{\mathrm{f_6}}^{\{\mathrm{i}\}}\bar{\mathrm{q}}_{\mathrm{f_6}}^{\{\mathrm{i}\}}]\\ \mathrm{m}^{\{\mathrm{i}\}}\dot{\delta}_0^2[\frac{1}{3}+\frac{1}{3}\bar{\mathrm{q}}_{\mathrm{f_4}}^{\{\mathrm{i}\}}]+2\mathrm{m}^{\{\mathrm{i}\}}\dot{\delta}_0[\frac{7}{20}\dot{\bar{\mathrm{q}}}_{\mathrm{f_5}}^{\{\mathrm{i}\}}-\frac{\mathrm{L_b}}{20}\dot{\bar{\mathrm{q}}}_{\mathrm{f_6}}^{\{\mathrm{i}\}}]\\ \mathrm{m}^{\{\mathrm{i}\}}\dot{\delta}_0^2[\frac{13}{35}\bar{\mathrm{q}}_{\mathrm{f_5}}^{\{\mathrm{i}\}}-\frac{11}{210}\mathrm{L_b}\bar{\mathrm{q}}_{\mathrm{f_6}}^{\{\mathrm{i}\}}]+2\mathrm{m}^{\{\mathrm{i}\}}\dot{\delta}_0[-\frac{7}{20}\dot{\bar{\mathrm{q}}}_{\mathrm{f_4}}^{\{\mathrm{i}\}}]\\ \mathrm{m}^{\{\mathrm{i}\}}\dot{\delta}_0^2[\frac{\mathrm{L_b^2}}{105}\bar{\mathrm{q}}_{\mathrm{f_6}}^{\{\mathrm{i}\}}-\frac{11}{210}\mathrm{L_b}\bar{\mathrm{q}}_{\mathrm{f_5}}^{\{\mathrm{i}\}}]+2\mathrm{m}^{\{\mathrm{i}\}}\dot{\delta}_0[\frac{\mathrm{L_b}}{20}\dot{\bar{\mathrm{q}}}_{\mathrm{f_4}}^{\{\mathrm{i}\}}]\end{array}\right\}. \tag{48}$$

As explained before, using the RFIM, the dynamics equations for the {i}-th flexible body is separated from those of the main rigid body subsystem of the SFFR depicted in Fig. 3. Also, the relationship between the generalized variables and the origin of the reference coordinates for the $\{i\}$th flexible body, or the two points on the rigid body can be written as:

$$\vec{\mathbf{R}}_{\mathrm{O}^{\{\mathrm{i}\}}}=\vec{\mathbf{R}}_{\mathrm{C}_0}+\vec{\mathbf{R}}_{\mathrm{O}^{\{\mathrm{i}\}}/\mathrm{C}_0}. \tag{49}$$

Differentiating this equation, the corresponding velocity and acceleration is obtained. These relationships must be considered in solving the rigid bodies dynamics together with the flexible subsystem. Therefore, we must first solve the dynamics equations of the rigid part of Eq. (40) to compute $\ddot{\mathbf{q}}$, $\dot{\mathbf{q}}$ and $\mathbf{q}$. Next, based on Eq. (49) and its derivatives, which establish the relationship between the generalized variables of the rigid SFFR and the generalized variables of the flexible members, we can compute $\ddot{\bar{\mathbf{q}}}_{\mathrm{r}}^{\{i\}}$, $\dot{\bar{\mathbf{q}}}_{\mathrm{r}}^{\{i\}}$ and $\bar{\mathbf{q}}_{\mathrm{r}}^{\{i\}}$. Then, these are used as the input terms in the equations of the flexible members to calculate $\ddot{\bar{\mathbf{q}}}_{\mathrm{f}}^{\{i\}}$, $\dot{\bar{\mathbf{q}}}_{\mathrm{f}}^{\{i\}}$ and $\bar{\mathbf{q}}_{\mathrm{f}}^{\{i\}}$. Finally, the inverse dynamics of the $\{i\}$th flexible body must be solved to compute $\mathbf{Q}_{\mathrm{e}}^{\{i\}}$ as:

$$\mathbf{M}_{\mathrm{f}}^{\{i\}}\ddot{\bar{\mathbf{q}}}^{\{i\}}+\mathbf{K}^{\{i\}}\bar{\mathbf{q}}^{\{i\}}=\mathbf{Q}_{\mathrm{e}}^{\{i\}}+\mathbf{Q}_{\mathrm{v}}^{\{i\}}. \tag{50}$$

Considering the last three equations of this equation, we can calculate the deformations of each flexible solar panel or $\bar{\mathbf{q}}_{\mathrm{f}}^{\{i\}}$. Next, we compute the forces of fixed end beam or the constraint forces $\mathbf{Q}_{\mathrm{e}}^{\{i\}}$as:

$$\mathbf{Q}_{\mathrm{e}}^{\{i\}}=\left\{\begin{array}{ccc}\mathrm{V}_{\mathrm{f_1}}^{\{i\}} & \mathrm{V}_{\mathrm{f_2}}^{\{i\}} & \mathrm{M}_{\mathrm{f_1}}^{\{i\}}\end{array}\right\}^{\mathrm{T}}. \tag{51}$$

So, we can calculate these forces using the first three equations of the inverse dynamics of the flexible body, which are exerted on the moving base as shown in Fig. 3:

$$\begin{aligned}\mathbf{Q}_{\mathrm{flex.}}^{\mathrm{x}}&=\mathrm{V}_{\mathrm{f_2}}^{\{\mathrm{L}\}}-\mathrm{V}_{\mathrm{f_2}}^{\{\mathrm{R}\}}\\ \mathbf{Q}_{\mathrm{flex.}}^{\mathrm{y}}&=\mathrm{V}_{\mathrm{f_1}}^{\{\mathrm{R}\}}-\mathrm{V}_{\mathrm{f_1}}^{\{\mathrm{L}\}}\\ \mathrm{M}_{\mathrm{flex.}}&=\left(\mathrm{M}_{\mathrm{f_1}}^{\{\mathrm{R}\}}+\mathrm{M}_{\mathrm{f_1}}^{\{\mathrm{L}\}}\right)-\left(\mathrm{V}_{\mathrm{f_2}}^{\{\mathrm{L}\}}+\mathrm{V}_{\mathrm{f_2}}^{\{\mathrm{R}\}}\right).(\mathrm{Lsin}(\pi/3))+\left(\mathrm{V}_{\mathrm{f_1}}^{\{\mathrm{L}\}}-\mathrm{V}_{\mathrm{f_1}}^{\{\mathrm{R}\}}\right).(\mathrm{Lcos}(\pi/3)),\end{aligned} \tag{52}$$

where $|\vec{\mathbf{R}}_{\mathrm{O}^{\{\mathrm{i}\}}/\mathrm{C}_0}|=\mathrm{L}$. Also, $\mathbf{Q}_{\mathrm{flex.}}(\beta_{\mathbf{0}})$ can be written as:

$$\mathbf{Q}_{\mathrm{flex.}}(\beta_{\mathbf{0}})=\left\{\begin{array}{ccc}\mathrm{Q}_{\mathrm{flex.}}^{\mathrm{x}} & \mathrm{Q}_{\mathrm{flex.}}^{\mathrm{y}} & \mathrm{M}_{\mathrm{flex.}}\end{array}\right\}^{\mathrm{T}}, \tag{53}$$

which completes the procedure of dynamics modeling of the complex SFFR system, using the introduced RFIM approach.

https://doi.org/10.1017/S0263574714002392 Published online by Cambridge University Press

Table I. The specifications of the flexible members [41].

$m = 9$ (Kg)	$\rho = 1.4$ (g/cm^3)
$L_b = 4$ (m)	$E = 60$ (GPa)
$a = 16$ (cm^2)	EI $= 20$ (N.m^2)

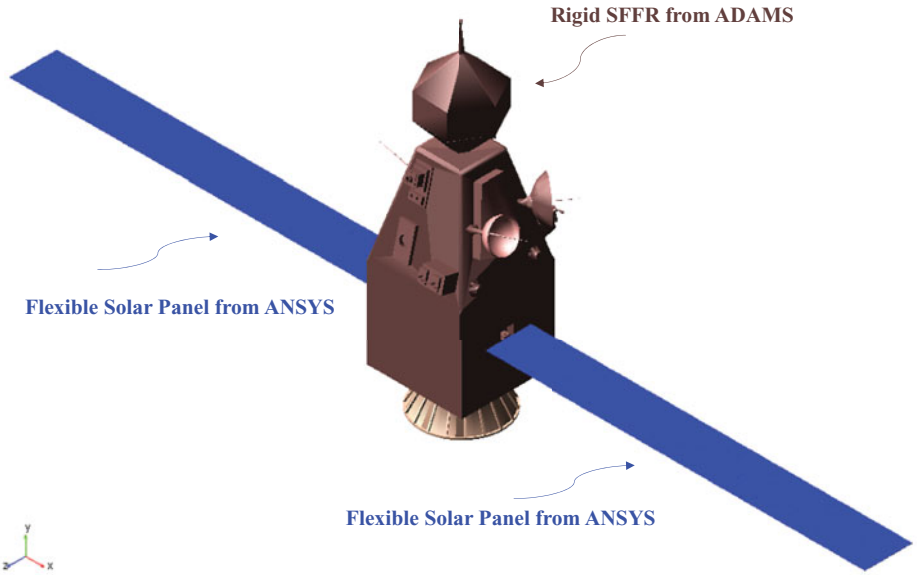

Fig. 4. The SFFR model in ADAMS and the flexible solar panels model from ANSYS.

5.2. Model verification

Verification of the rigid model of SFFR has been already discussed in comparison with other methods.[36] So, the main focus should be on the model augmentation with the flexible parts, where the corresponding parameters are described in Table I. The verification procedure is completed through comparisons between the responses of the obtained model using the proposed RFIM approach, and those obtained from a comprehensive routine based on a combination usage of ADAMS (for analysis of rigid parts) and ANSYS (for precise analysis of flexible modes). Each flexible member is modeled as a beam with the specified parameters given in Table I, using SOLID45 element in ANSYS. Next, this model is exported from ANSYS to ADAMS software while attached to the solid parts (Fig. 4). Then, a known force is applied to the main rigid body, and the response of this model is compared to that of the developed explicit model based on RFIM to verify the dynamics model of the assumed robot.[35] As a typical comparison result, Fig. 5 shows the tip displacement of flexible solar panels. It can be seen that the proposed RFIM modeling approach leads to absolutely exact results, even for this highly complex system. Also, despite accumulative dynamics approach, the effects of various terms in the dynamics of rigid–flexible multi-body systems can be observed separately and studied. Therefore, the RFIM approach can accurately model the system dynamics while the simplicity of the model computations will be significantly helpful for both control analysis and synthesis.

5.3. Obtained results

The geometric and mass parameters for the two solar panels are described in Table I, and those of the main rigid base are given in Table II. The mechanical characteristics of piezoelectric patches that are mounted on the panels (as introduced in Eq. (15)) are described in Table III chosen from related literature,[42] and the initial conditions are described in Table IV. Note that the mass of these piezoelectric actuators compared to the mass of the flexible solar panels is negligible. An operation along a circular path is considered with a radius of 15 m. As shown in Fig. 6, a comparison between the AHSC and HSC algorithms was performed by considering the force controlling of the flexible solar panels, while the same conditions are considered for both algorithms. As it is seen in this figure,

https://doi.org/10.1017/S0263574714002392 Published online by Cambridge University Press

Table II. The geometric and mass parameters of the assumed SFFR system.

i,j $i=1$ j	$i=2$	m_{ij} (kg)	1 (m)	$I_{Z_{ij}}$(kg.m^2)
0		**50**	**1**	**10**
1		**4**	**1**	**0.5**
2		**3**	**1**	**0.5**

Table III. Mechanical characteristics of the actuators on flexible members[34].

Actuators	Max. Force (N)	Stiffness (N.m^{-1})	Mass (kg)
PZT	47.5	9.30×10^5	2.6×10^{-2}

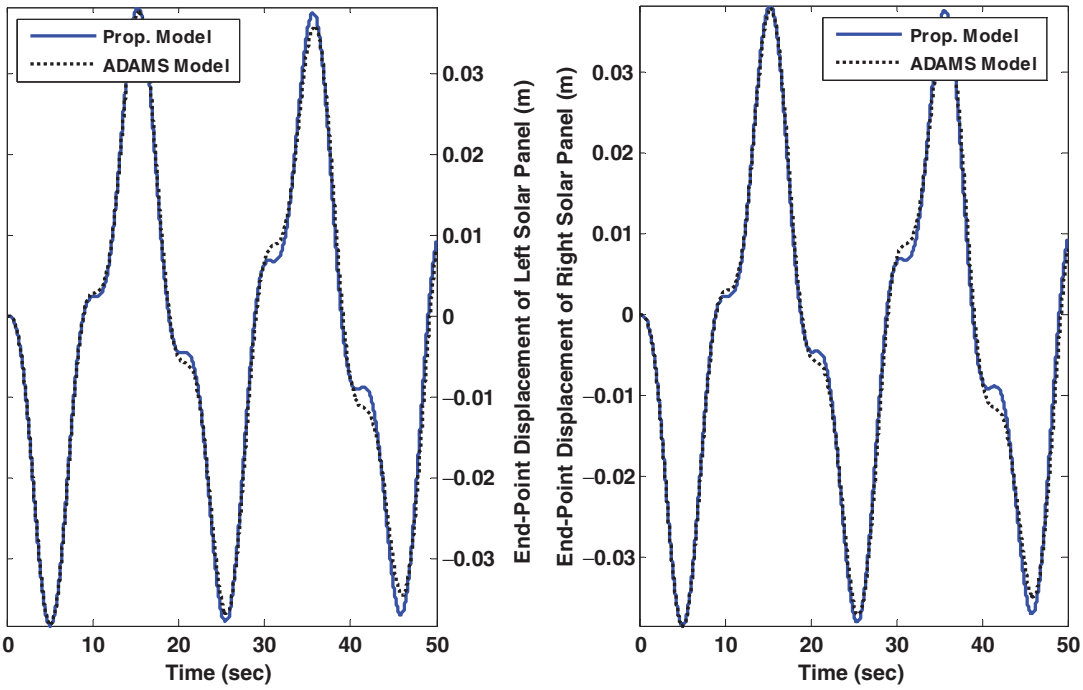

Fig. 5. Response comparison of the obtained model for SFFR, and the one developed in ADAMS/ANSYS.

the proposed adaptation law of AHSC can significantly decrease the vibrations of the solar panels by changing the virtual damping, compared to HSC, see Fig. 7. Figs. 8 and 9 show that the proposed AHSC algorithm can successfully perform the task while the virtual damping quantity of each flexible solar panel is modified using the designed adaptation law. As shown in these figures, almost a perfect tracking is obtained as the errors and their rates converge to zero. The corresponding generalized forces acting on the robot base and the links are shown in Figs. 10 and 11. As mentioned before, we assume that hot continuous thrusters are acting on the base. Furthermore, the considered saturation band for these thrusters, and the joint actuators are defined as 100 (N) and 7 (N.m), respectively. It should be noted that we have deliberately imposed an initial speed to the flexible solar panels as shown in Fig. 12. This is done to excite the flexible solar panels, and consequently the performance of this active controller can be studied more precisely. Simulation results show that even though the object manipulation operation excites vibration of the solar panels, the AHSC can successfully control these undesirable oscillations. The time history of aforementioned deflections is shown in Fig. 12 for a few time steps. Finally, an animated view of the system performing the object manipulation task along the desired circular path is shown in Fig. 13.

https://doi.org/10.1017/S0263574714002392 Published online by Cambridge University Press

Table IV. Initial conditions for the case study.

$\mathbf{q}(0) = [0\ 0\ 0\ 0.6\ 4.2\ 5.6\ 2.1\ \pi/7\ \pi/36]^{\mathrm{T}}$	$\dot{\mathbf{q}}(0) = [0.85\ 0\ 0\ 0\ 0\ 0\ 0\ 0\ 0]^{\mathrm{T}}$
$\tilde{\mathbf{q}}_{\mathrm{f}}(0) = \begin{bmatrix} 0\ 0\ 0 \end{bmatrix}^{\mathrm{T}}$	$\dot{\tilde{\mathbf{q}}}_{\mathrm{f}}(0) = \begin{bmatrix} 0\ -0.1\ 0 \end{bmatrix}^{\mathrm{T}}$
$\hat{\mathbf{B}}^{\{\mathrm{i}\}}_{\mathrm{f}_{\mathrm{virtual}}}(0) = \begin{bmatrix} 3500\ 1.5\ 5 \end{bmatrix}^{\mathrm{T}}$	$\Gamma_1 = 700, \Gamma_2 = 10, \Gamma_3 = 15$
$K_{\mathrm{p}}{=}\tilde{K}_{\mathrm{p}}{=}900$	$K_{\mathrm{d}}{=}\tilde{K}_{\mathrm{d}}{=}300$

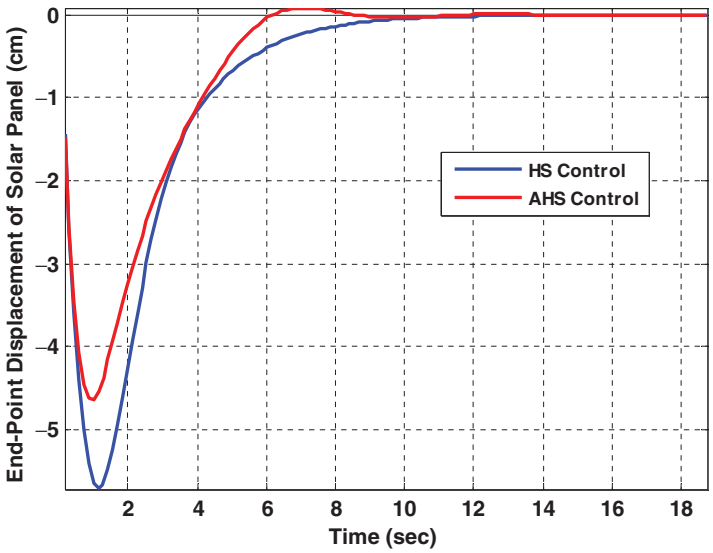

Fig. 6. A comparison between the AHS Control and HS Control operation during the cooperative object manipulation.

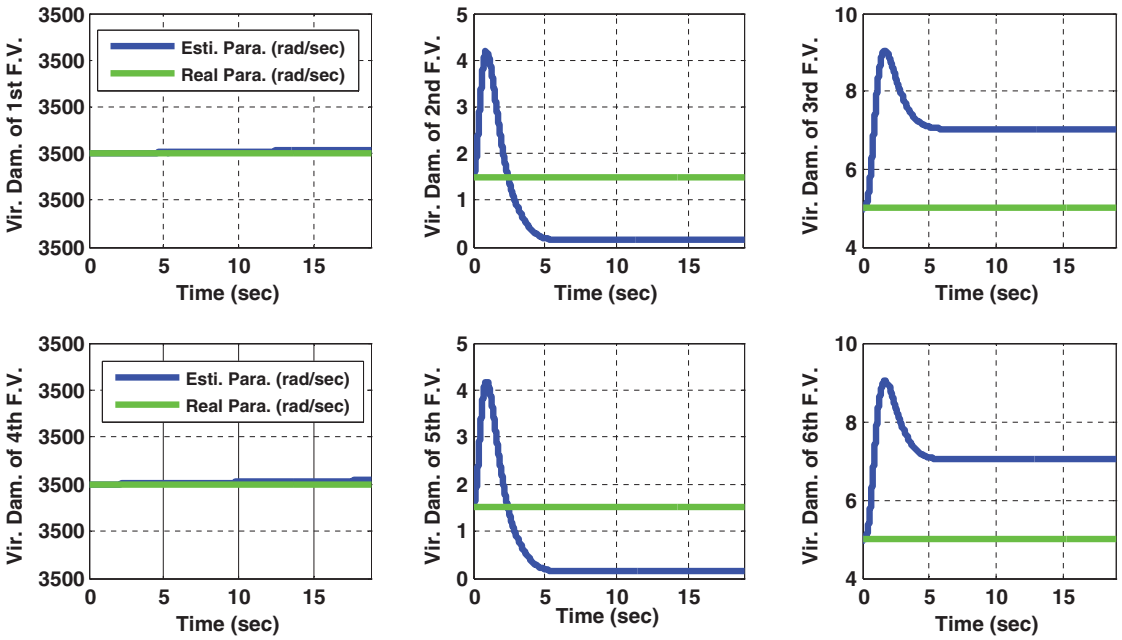

Fig. 7. Changing in virtual damping of left and right flexible solar panels.

6. Conclusions

In this article, AHSC of cooperative object manipulation by rigid–flexible multi-body systems was proposed. To this end, first the RFIM approach for dynamics modeling of such systems was

https://doi.org/10.1017/S0263574714002392 Published online by Cambridge University Press

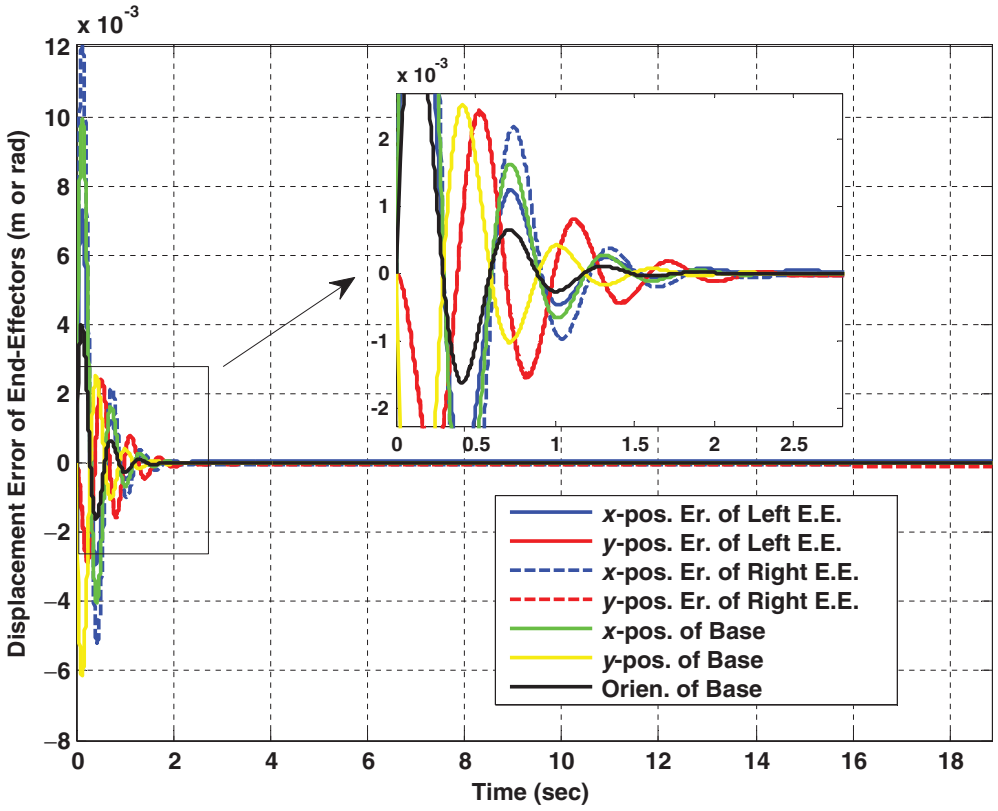

Fig. 8. Error of the work space variables during the cooperative object manipulation task.

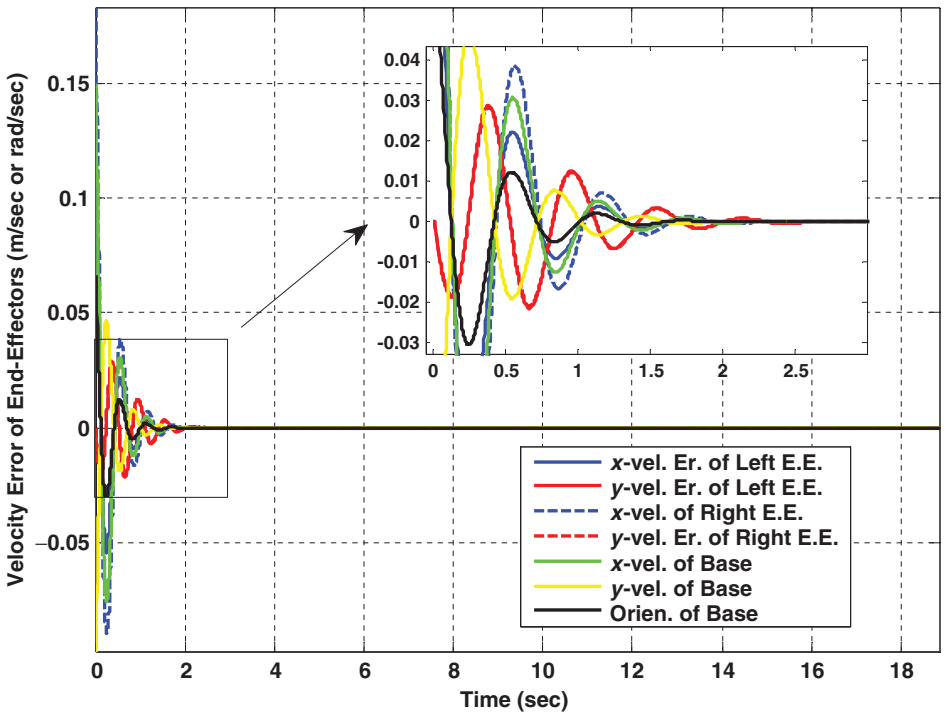

Fig. 9. Error of the work space variables rates during the cooperative object manipulation task.

https://doi.org/10.1017/S0263574714002392 Published online by Cambridge University Press

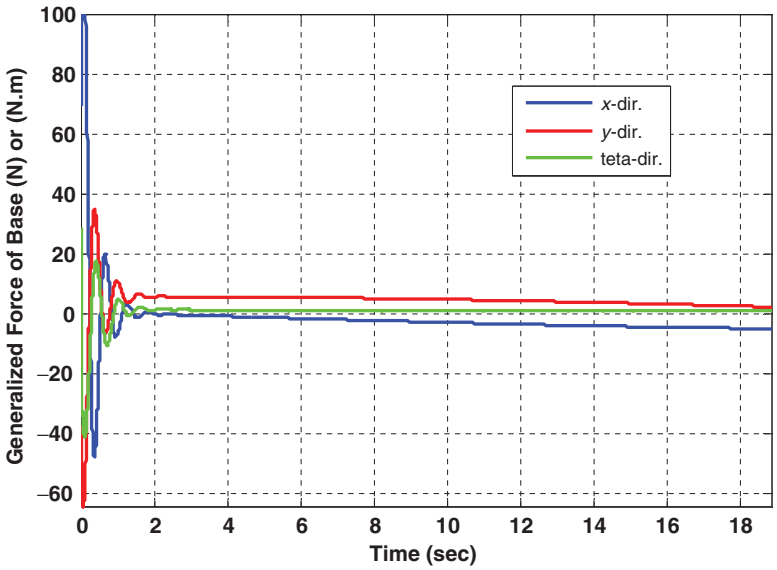

Fig. 10. Generalized force of robot actuators during the cooperative object manipulation task.

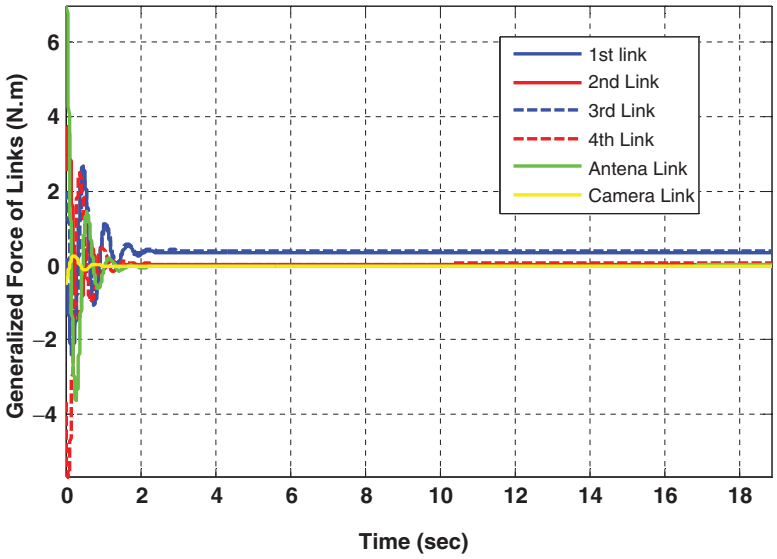

Fig. 11. Generalized force of link actuators during the cooperative object manipulation task.

studied. Using the RFIM approach, the motion equations of rigid and flexible members are separately developed, then assembled and solved simultaneously at each time step by considering the mutual interaction and constraint forces. Therefore, the compact dynamics model, obtained using the RFIM approach, is extremely useful for control design and simulation studies, and also for practical implementations. Using the proposed dynamics model, an HSC algorithm was presented. It was emphasized that control of such systems is highly complicated due to severe under-actuated condition caused by flexible elements, and an inherent uneven nonlinear dynamics. Next, the AHSC algorithm was developed in which the virtual damping is computed based on a designated adaptation law, and its stability and the error convergence were proven. Finally, to reveal the merits of the proposed control algorithm, its application on a SFFR system was studied. Obtained results of the model verification and implementation of the proposed controllers on the rigid–flexible multi-body system were discussed. It was shown that vibration of the flexible solar panels results in reaction forces

https://doi.org/10.1017/S0263574714002392 Published online by Cambridge University Press

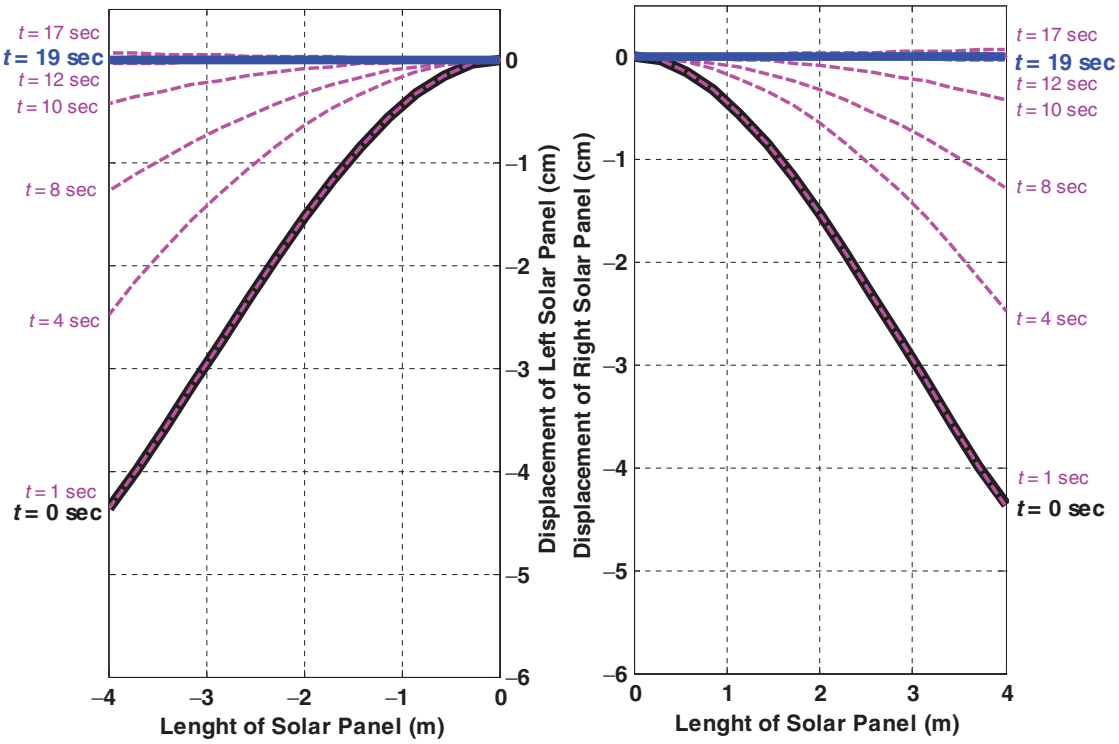

Fig. 12. Deflection time history of the flexible solar panels using the AHSC algorithm.

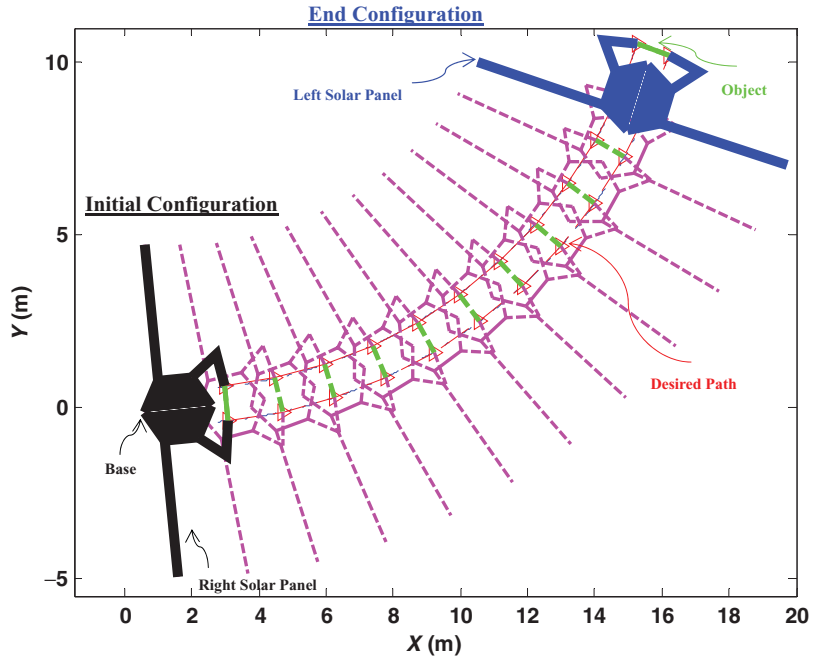

Fig. 13. An animated view of the system during the cooperative object manipulation.

on the moving base which can produce undesirable errors of the end-effectors. These effects were significantly eliminated by the application of the proposed AHSC algorithm, while the manipulation task was successfully performed.

https://doi.org/10.1017/S0263574714002392 Published online by Cambridge University Press

References

1. S. Moosavian, A. Ali and E. Papadopoulos, "Free-flying robots in space: An overview of dynamics modelling, planning and control," *J. Robot.* **25**, 537–547 (2007).
2. S. K. Dwivedy and P. Eberhard, "Dynamic analysis of flexible manipulators, a literature review," *J. Mech. Mach. Theory* **41**, 749–777 (2006).
3. M. McConley, "Review of stability and control of large-scale dynamical systems: A vector dissipative systems approach," *AIAA J. Guid. Control Dyn.* **35**(5), 1688–1689 (2012).
4. P. Zarafshan, S. Moosavian and A. Ali, "Control of a Space Robot with Flexible Members," *Proceedings of the IEEE International Conference on Robotics and Automation (ICRA2011)*, Shanghai, China, (2011) pp. 2211–2216.
5. A. A. Ata and H. Johar, "Dynamic Force/Motion Simulation of a Rigid Flexible Manipulator during Task Constrained," *Proceedings of the IEEE International Conference on Mechatronics*, (2004) pp. 268–273.
6. K. Yoshida, H. Nakanishi, H. Ueno, N. Inaba, T. Nishmaki and M. Oda, "Dynamics, control and impedance matching for robotic capture of a non-cooperative satellite," *J. Adv. Robot.* **18**(2), 175–198 (2004).
7. M. Sabatinia, P. Gasbarrib, R. Montib and G. B. Palmerinia, "Vibration control of a flexible space manipulator during on orbit operations," *Acta Astronaut.* **73**, 109–121 (2012).
8. A. Fattah, J. Angeles and A. K. Misra, "Dynamics of a 3-DOF Spatial Parallel Manipulator with Flexible Links," *Proceedings of the IEEE International Conference on Robotics and Automation*, (1995) pp. 627–632.
9. S. Kasai and H. Kojma, "Input-shaped link motion control of planar space robot equipped with flexible appendage," *Trans. Japan Soc. Aeronaut. Space Sci.* **55**(4), 205–213 (2012).
10. S. Ulrich, Z. J. Sasiadek, and I. Barkana, "Modeling and direct adaptive control of a flexible-joint manipulator," *AIAA J. Guid. Control Dyn.* **35**(1), 25–39 (2012).
11. P. Zarafshan, and S. A. A. Moosavian, "Cooperative object manipulation by a space robot with flexible appendages," *J. ISRN Aerosp. Eng.* 2013, Article ID 965481, 1–14 (2013).
12. P. Zarafshanand S. A. A. Moosavian, "Dynamics modelling and hybrid suppression control of space robots performing cooperative object manipulation," *J. Commun. Nonlinear Sci. Numer. Simul.* **18**(10), 2807–2824 (2013).
13. P. Zarafshan and S. A. A. Moosavian, "Adaptive Hybrid Suppression Control of a Wheeled Mobile Robot with Active Flexible Members," *Proceedings of the IEEE International Conference on Mechatronics and Automation (ICMA 2011)*, Beijing, China, (2011), pp. 932–937.
14. A. A. Shabana, *Dynamics of Multi-Body Systems*, 3rd ed. (Cambridge University Press, Cambridge 2005), Chaps. 4–6.
15. R. Jain and P. M. Pathak, "Trajectory planning of 2 DOF planar space robot without attitude controller," *World J. Modelling Simul.* **4**(3), 196–204 (2008).
16. A. Suleman, "Multibody dynamics and nonlinear control of flexible space structures," *J. Vib. Control* **10**(11), 1639–1661 (2004).
17. X. Zhang, W. Xu, S. S. Nair and V. S. Chellabonia, "PDE modeling and control of a flexible two-link manipulator," *IEEE Trans. Control Syst. Technol.* **13**(2), 301–312 (2005).
18. O. Zer and S. E. Semercigil, "An event-based vibration control for a two-link flexible robotic arm: Numerical and experimental observations," *J. Sound Vib.* **31**(3), 375–394 (2008).
19. S. Kilicaslana, M. K. Ozgörenb and S. K. Iderb, "Hybrid force and motion control of robots with flexible links," *J. Mech. Mach. Theory* **45**(1), 91–105 (2010).
20. Z. H. Jiang, "Impedance control of flexible robot arms with parametric uncertainties," *J. Intell. Robot. Syst.* **42**(2), 113–133 (2005).
21. S. Moosavian, A. Ali, R. Rastegari and E. Papadopoulos, "Multiple impedance control for space free-flying robots," *AIAA J. Guid. Control Dyn.* **28**(5), 939–947 (2005).
22. R. Holmberg and O. Khatib, "Development and control of a holonomic mobile robot for mobile manipulation tasks," *Int. J. Robot. Res.* **19**(11), 1066–1074 (2002).
23. S. Moosavian, A. Ali and H. R. Ashtiani, "Cooperation of robotic manipulators using non-model-based multiple impedance control," *J. Ind. Robot.* **35**(6), 549–558 (2008).
24. X. Ge and Y. Liu, "The attitude stability of a spacecraft with two flexible solar arrays in the gravitational field," *J. Chaos Solitons Fractals* **37**, 108–112 (2008).
25. B. Pratiher and S. K. Dwivedy "Non-linear dynamics of a flexible single link cartesian manipulator," *Int. J. Non-Linear Mech.* **42**, 1062–1073 (2007).
26. J. A. C. Ambrosio, "Dynamics of structures undergoing gross motion and nonlinear deformations: a multi-body approach," *J. Comput. Struct.* **59**(6), 1001–1012 (1996).
27. C. Schmitke and J. McPhee, "Using linear graph theory and the principle of orthogonality to model multi-body, multi-domain systems," *J. Adv. Eng. Inform.* **22**(2), 147–160 (2008).
28. M. J. Sadigh and A. K. Misra, "Stabilizing Tethered Satellite Systems Using Space Manipulators," *Proceedings of the IEEE International Conference on Intelligent Robots and Systems*, (1994) pp. 1546–1553.
29. H. Zohoor and S. M. Khorsandijou, "Dynamic model of a flying manipulator with two highly flexible links," *J. Appl. Math. Modelling* **32**, 2117–2132 (2008).
30. J. F. Deu, A. C. Galucio and R. Ohayon, "Dynamic responses of flexible-link mechanisms with passive/active damping treatment," *J. Comput. Struct.* **86**, 258–265 (2008).

31. K. S. Anderson and S. Duan, "A hybrid parallelizable low-order algorithm systems for dynamics of multi-rigid-body part I, chain systems," *Math. Comput. Modell.* **30**, 193–215 (1999).
32. J. J. McKetta, "Coupling of Substructures for Dynamic Analyses: An Overview," *AIAA J. -1573*, (2000).
33. B. Simeon, "On lagrange multipliers in flexible multi-body dynamics," *Comput. Methods Appl. Mech. Eng.* **195**, 6993–7005 (2006).
34. B. Subudhi and A. S. Morris, "Soft computing methods applied to the control of a flexible robot manipulator," *Appl. Soft Comput.* **9**, 149–158 (2009).
35. P. Zarafshan, S. Moosavian, and A. Ali, "Rigid-flexible interactive dynamics modelling approach," *J. Math. Comput. Modell. Dyn. Syst.* **18**(2), 1–25 (2011).
36. R. Siegwart and I. R. Nourbakhsh, *Introduction to Autonomous Mobile Robots* (Prentice-Hall of India, New Delhi, India, 2005), Chaps. 1, 2, 3.
37. V. Piefort, "Finite element modelling of piezoelectric active structures," *Ph.D. Thesis*, (Faculty of Applied Sciences, University of Libre De Bruxelles, 2001).
38. G. S. Aglietti, R. S. Langley, S. B. Gabriel and E. Rogers, "A modeling technique for active control design studies with application to spacecraft microvibrations," *J. Acoust. Soc. Am.* **102**(4), 2158–2166 (1997).
39. J. J. E. Slotine and W. Li, *Applied Nonlinear Control* (Prentice Hall, Englewood Cliffs, NJ, 1991), Chap. 6.
40. S. Moosavian, A. Ali and E. Papadopoulos, "Explicit dynamics of space free-flyers with multiple manipulators via SPACEMAPLE," *J. Adv. Robot.* **18**(2), 223–244 (2004).
41. V. R. Katti, K. Thyagarajan, K. N. Shankara and A. S. Kiran Kumar, "Spacecraft technology," *J. Curr. Sci.* **93**(12), 1715–1736 (2007).
42. M. J. Brennan, J. G. Bonito, S. J. Elliott, A. David and R. J. Pinnington, "Experimental investigation of different actuator technologies for active vibration control," *J. Smart Mater. Struct.* **8**, 145–153 (1999).